

3 **Towards a more reliable historical reanalysis:**
4 **Improvements for version 3 of the Twentieth**
5 **Century Reanalysis system**

6 **Laura C. Slivinski et. al.^{1,2}**

¹U. of CO Cooperative Institute for
Research in Environmental Sciences,
7 Boulder, CO, USA

²NOAA Earth System Research Laboratory,
Boulder, CO, USA

Correspondence

Laura C. Slivinski, NOAA/ESRL Physical
Sciences Division, 325 Broadway, Boulder,
CO, 80305, USA
Email: laura.slivinski@noaa.gov

Funding information

Historical reanalyses that span more than a century are

This is the author manuscript accepted for publication and has undergone full peer review but has not been through the copyediting, typesetting, pagination and proofreading process. This may lead to differences between this version and the Version of Record. Please cite this article as doi: [10.1002/qj.3598](https://doi.org/10.1002/qj.3598)

needed for a wide range of studies, from understanding

Author Manuscript

8

large-scale climate trends to diagnosing the impacts of in-

Author Manuscript

dividual historical extreme weather events. The Twentieth Century Reanalysis (20CR) Project is an effort to fill this need. It is supported by the National Oceanic and Atmospheric Administration (NOAA), the Cooperative Institute for Research in Environmental Sciences (CIRES), and the Department of Energy (DOE), and is facilitated by collaboration with the international Atmospheric Circulation Reconstructions over the Earth initiative. 20CR is the first ensemble of sub-daily global atmospheric conditions spanning over 100 years. This provides a best estimate of the weather at any given place and time as well as an estimate of its confidence and uncertainty. While extremely useful, version 2c of this dataset (20CRv2c) has several significant issues, including inaccurate estimates of confidence and a global sea level pressure bias in the mid-19th century. These and other issues can reduce the effectiveness of studies at many spatial and temporal scales. Therefore, the 20CR system underwent a series of developments to generate a significant new version of the reanalysis. The version 3 system (NOAA-CIRES-DOE 20CRv3) uses upgraded data assimilation methods including an adaptive inflation algorithm; has a newer, higher-resolution forecast model that specifies dry air mass; and assimilates a larger set of pressure observations. These changes have improved the ensemble-based estimates of confidence, removed spin-up effects in the precipitation fields, and diminished the sea level pressure bias. Other improvements include more accurate representations of storm intensity, smaller errors, and large-scale reductions in model bias. The 20CRv3 system is comprehensively reviewed, focusing on the aspects that have ameliorated issues in 20CRv2c. Despite the many improvements, some challenges remain, including a systematic bias in tropical precipitation and time-varying biases in southern high latitude pressure fields.

KEYWORDS

reanalysis, data assimilation, surface pressure

11 **Full author list** (*Affiliations provided separately.*)

12 Laura C. Slivinski et. al.
13 Gilbert P. Compo
14 Jeffrey S. Whitaker
15 Prashant D. Sardeshmukh
16 Benjamin S. Giese
17 Chesley McColl
18 Rob Allan
19 Xungang Yin
20 Russell Vose
21 Holly Titchner
22 John Kennedy
23 Lawrence J. Spencer
24 Linden Ashcroft
25 Stefan Brönnimann
26 Manola Brunet
27 Dario Camuffo
28 Richard Cornes
29 Thomas A. Cram
30 Richard Crouthamel
31 Fernando Domínguez-Castro
32 J. Eric Freeman
33 Joëlle Gergis
34 Ed Hawkins
35 Philip D. Jones
36 Sylvie Jourdain
37 Alexey Kaplan
38 Hisayuki Kubota
39 Frank Le Blancq
40 Tsz-Cheung Lee
41 Andrew Lorrey
42 Jürg Luterbacher
43 Maurizio Maugeri
44 Cary J. Mock
45 G.W. Kent Moore
46 Rajmund Przybylak
47 Christa Pudmenzky
48 Chris Reason
49 Victoria C. Slonosky
50 Cathy Smith
51 Birger Tinz
52 Blair Trewin
53 Maria Antónia Valente

- 54 Xiaolan L. Wang
55 Clive Wilkinson
56 Kevin Wood
57 Przemysław Wszyński

Author Manuscript

1 | INTRODUCTION

In order to study historical and contemporary weather events including extremes within a broader climate context, long time series of accurate, reliable, sub-daily atmospheric variables are essential. Retrospective analyses, or 'reanalyses', take advantage of the benefits of past observations and modern weather forecast models by combining the two in a process called 'data assimilation' (DA; Daley (1993)). The idea of 'reanalysis' arguably began in the early 19th century with Brandes' hand-drawn synoptic weather maps (Monmonier, 1999), and has matured significantly in the centuries since; see Compo et al. (2006) and Compo et al. (2011) for a detailed history. Historical reanalyses, which span a century or longer, act as a bridge between weather and climate since they are intended to capture individual weather events around the globe as well as larger climatic trends over many decades within the context of a single, consistent dataset (Slivinski, 2018).

In contrast to historical reanalyses, 'modern' reanalyses generally only extend back to the 1950s, and more often only to 1979, when upper-air and satellite data are available for assimilation. These reanalyses include the European Centre for Medium-Range Weather Forecasts (ECMWF) interim Re-Analysis ERA-Interim (Dee et al., 2011), the National Aeronautics and Space Administration (NASA) Modern-Era Retrospective analysis for Research and Applications version 2 (MERRA-2) (Gelaro et al., 2017), the 55-year Japanese Re-Analysis JRA-55 (Kobayashi et al., 2015), and the reanalysis produced jointly by the US National Centers for Environmental Prediction (NCEP) and the National Center for Atmospheric Research (NCAR), the NCEP-NCAR Reanalysis (Kalnay et al., 1996; Kistler et al., 2001), among others (see Fujiwara et al. (2017) for a review of reanalysis systems). At present, long-term studies using modern reanalyses are restricted to span as few as 40-60 years, preventing in-depth investigation of infrequent extreme weather and climate events. Another difficulty is that significant changes to the observing system, such as the introduction of satellite data, can yield non-climatic discontinuities in some reanalysis fields, including an apparent shift in tropical divergent circulation (Kinter III et al., 2004) and trends in temperature, integrated water vapor, kinetic energy, and precipitation (Bengtsson et al., 2004; Bosilovich et al., 2011; Zhang et al., 2012). In order to avoid such artifacts, historical reanalyses that span at least a century assimilate only near-surface conventional observations, which have been available for the entire time period: specifically, surface pressure and marine winds.

The NOAA-CIRES Twentieth Century Reanalysis (20CR) marked the introduction of recent efforts to generate historical reanalyses, as it was the first reanalysis to assimilate only surface pressure observations (Compo et al., 2011). Since then, the range of studies to use these types of data has grown, and other centennial reanalyses were developed that assimilated these data. ECMWF produced ERA-20C (Poli et al., 2016), an atmospheric reanalysis spanning 1900 to 2010 that assimilated surface pressure as well as marine winds, and CERA-20C (Laloyaux et al., 2018), which utilizes a coupled ocean-atmosphere model and spans 1901 to 2010. In addition, NOAA and CIRES produced an update to the 20CR version 2 described by Compo et al. (2011) that spanned 1871 to 2012; this update, 20CR version 2c (20CRv2c; see Giese et al. (2016) and detailed below), extended back to 1851 and ameliorates several issues with 20CRv2. Finally, the latest 20CR version 3 (20CRv3) is currently being produced by NOAA, CIRES, and DOE. It is expected to extend back to 1836 and to be released in 2019.

Historical reanalyses have broad areas of application because they span timescales of weather to climate by providing sub-daily estimates of the Earth system with global coverage for a century or longer. These datasets have been utilized in studies including: climate change (e.g. Compo et al. (2013); Huang et al. (2016)); climate dynamics (e.g. Huang et al. (2017)); trends in hurricanes (e.g. Burn and Palmer (2015)), extra-tropical cyclones (e.g. Wang et al. (2013, 2016)), and extremes in temperature and precipitation (e.g. Donat et al. (2016)); blocking (e.g. Häkkinen et al. (2011); Rohrer et al. (2018)); individual case studies of particular storms (e.g. Moore and Babij (2017)); historic climatology in remote regions (e.g. Lorrey and Chappell (2016)); El Niño (e.g. Giese et al. (2010); Deser et al. (2017)); the Madden-Julian

100 Oscillation (e.g. Klotzbach et al. (2016)); convergence zone activity (e.g. Lorrey et al. (2012); Harvey et al. (2019));
101 seasonal and climatic responses to volcanic eruptions (e.g. Brohan et al. (2016); Paik and Min (2017)); weather typing
102 (e.g. Jones et al. (2013, 2016)); and the emerging field of decadal climate prediction (e.g. Mueller et al. (2014)), among
103 many others.

104 A key aspect for informed application of reanalyses is properly accounting for their uncertainty (e.g. Parker (2016)).
105 Comparing different reanalyses that span similar time periods is one way to cross-validate the datasets and determine a
106 'meta-confidence' by agreement or disagreement among the datasets. It is also important that each historical reanalysis
107 dataset is as accurate as possible, both in terms of past climate state estimates as well as internal quantification of
108 its uncertainty (as measured by ensemble standard deviation or 'spread', for instance). This internal quantification of
109 uncertainty is used by the data assimilation system during the production of the reanalysis to make the best use of the
110 observations and prior background information, but is also important to the end-users of the reanalysis. As an example,
111 a historical reanalysis may display a long-term trend in one variable that, according to the quantified uncertainty of
112 the dataset, is significant. However, researchers may be unaware that the trend is an artificial one due to a bias in the
113 observations, and appears to be significant solely due to errors in the uncertainty estimate. Continuing to work towards
114 more reliable historical reanalyses allows studies on all timescales, such as those listed above, to avoid erroneous
115 conclusions and make use of the best data possible.

116 In this vein, despite several major improvements from 20CRv2 to 20CRv2c, certain issues remain. While some are
117 obvious, such as artificial large-scale trends and a lack of certain major storm systems, others are more subtle, such as
118 suboptimal usage of observations and inaccurate estimates of confidence. These problems can hinder the effectiveness
119 of 20CRv2c for climate analysis applications. Investigations into many of these issues occurred prior or in parallel to
120 development of version 3, informing the implementation of particular algorithms that are expected to improve the
121 efficacy of the reanalysis. In other cases, version 3 will likely benefit from general improvements and upgrades to the
122 system, as well as a larger observational database. This work discusses how the significant issues in version 2c are
123 addressed, as well as other upgrades to the version 3 system. Preliminary results with the 20CRv3 dataset shown here
124 will focus on several test periods between 1851 and 2002, and are intended to be representative of different time
125 periods (in terms of quality, confidence, observational network density, biases, etc.) Results from the complete 20CRv3
126 dataset and deeper investigations of it on climatic and synoptic scales are left for future works. Unless otherwise noted,
127 all maps shown below are plotted at the native resolution of the dataset. Finally, we emphasize that many updates to
128 the 20CRv3 system were made simultaneously, so a single improvement in this preliminary 20CRv3 data can rarely be
129 attributed to a specific change in the system.

130 The Twentieth Century Reanalysis system is described in detail in Section 2. Aspects of the system that changed
131 from 20CRv2c to 20CRv3 are highlighted, as well as features of the version of the NCEP Global Forecast System (GFS)
132 coupled atmosphere-land model used. Section 3 discusses several large-scale issues in the confidence derived from
133 ensemble spread and in the biases of sea level pressure (SLP), precipitation, and wind in 20CRv2c. Preliminary results
134 suggest that updates to the forecast model and data assimilation algorithm will improve the confidence estimation
135 and reduce most of these biases in 20CRv3. In addition to addressing known issues, other developments in the
136 version 3 system are expected to result in further improvements. As shown in Section 4, updates to the localization
137 procedure, quality control, and observation errors will likely improve the use of observations and result in more accurate
138 representations of variability and extremes, such as tropical cyclones. Despite significant improvements across the
139 board, several issues remain in the 20CRv3 system. These are discussed in Section 5. Section 6 concludes with a
140 discussion and final remarks.

2 | SYSTEM OVERVIEW

In several basic ways, each iteration of the Twentieth Century Reanalysis system remains the same as that proposed originally by Compo et al. (2006). First, modern weather forecast models are used to generate the atmospheric background fields given prescribed sea surface temperature (SST) and sea ice concentration fields. Second, an ensemble method assimilates historical observations to update the background fields, yielding analysis fields. Ensemble methods are particularly useful as they allow for estimates of uncertainty and confidence via ensemble spread (e.g., ensemble standard deviation) as well as an estimate of the atmospheric state via the ensemble mean. Finally, surface pressure values are the only type of observations that are ever assimilated. Sea ice and SST observations are implicitly included in the reanalysis in the form of boundary conditions and can guide the model to represent large-scale climate features, but they are not assimilated. While the temporal frequency, spatial density, and quality of the surface pressure observations have changed over time as a result of developments in instrumentation and theory (Middleton, 1964), the 20CR system assumes that the most important part of the observation error is its so-called ‘error of representativeness’ (Lorenz, 1986; Janjić and Cohn, 2006). Observation errors are therefore assumed to be constant in time; see Section 4.2 for more discussion. Feedback from reanalysis datasets that assimilate these observations can be used to improve this estimate in the future (e.g., Poli et al. (2015); Laloyaux et al. (2018)).

For purposes of comparison, the 20CRv2c system outlined by Giese et al. (2016) is detailed in Appendix A, and the 20CRv3 system is detailed here. To address significant issues in the 20CRv2c dataset, and as a result of general progress in the fields of modeling and data assimilation, several aspects of the 20CR system were updated before producing 20CRv3. Broadly, 20CRv3 will benefit from an improved, higher-resolution model; a larger observational database; updated data assimilation methods; and a larger ensemble size. The atmospheric model used in 20CRv3 has been updated to the 2017 version of the NCEP GFS with a resolution of total spherical wavenumber 254 (about 0.5 deg. horizontal resolution) and 64 vertical hybrid sigma-pressure levels; differences between the version of the GFS operational in fall 2017 and the version used for 20CRv3 are detailed in Appendix A. Additionally, the version 2c system allowed the assimilation to update the dry air pressure, resulting in a feedback loop with biased observations that caused significant artificial trends in the mid-19th century; see Section 3. In version 3, the dry air pressure was held fixed in the forecast and analysis steps.

The 20CRv2c dataset began in 1851 due to the availability of its prescribed sea ice fields. The addition of more 19th century observations available to the 20CRv3 assimilation system, as well as early investigations of confidence and forecast errors (not shown), suggested that 20CRv3 could span further back in time than 20CRv2c, given appropriate boundary conditions. 1804 is the first year that every 6-hour window has at least one observation (globally) to be assimilated. Due to computational and storage resource limitations, 1836 was the earliest year that 20CRv3 could be produced. Experiments for the years 1804-1835 are ongoing.

The 20CRv3 dataset is expected to consist of two overlapping sub-versions: 20CRv3si (1836–2012) and 20CRv3mo (1981–2015), where the only difference between the two sub-versions is the prescribed SSTs. 20CRv3mo prescribes SSTs from HadISST2.2 (Rayner et al., 2006; Poli et al., 2016; Laloyaux et al., 2018), which consists of an ensemble of 5-day average SST fields interpolated to daily resolution. This interpolation is cubic, with the coefficients adapted to the autocorrelation of the data (Kwon et al., 2004). Of the 10 members available, two of the ensemble members had quite different bias adjustments from the others; thus, 20CRv3mo only uses the remaining 8 members as boundary conditions. 20CRv3si prescribes SSTs from the pentad, linearly interpolated to daily, 8-member Simple Ocean Data Assimilation with sparse input version 3 (SODAsi.3) ensemble that itself used 20CRv2c fields as atmospheric boundary conditions and forcing (Giese et al., 2016). The SODAsi.3 SSTs used for 20CRv3si were seasonally adjusted to the 1981–2010 HadISST2.2 daily climatology. For both versions, each of the 8 distinct SST ensemble members was duplicated 10 times

183 to create a total of 80 members. Thus, the first, 9th, 17th, 25th, ..., and 73rd members of the 20CRv3 ensemble have the
184 same SST forcing, and the second, 10th, 18th, 26th, ..., and 74th members have the same SST forcing as each other (but
185 different from the first set), and so on. Sea ice concentrations were specified from HadISST2.3, which is identical to
186 HadISST2.2 (Titchner and Rayner, 2014) from 1972 onwards. From 1850 to 1971, HadISST2.3 specifies Arctic sea ice
187 extent from the Sea Ice Back To 1850 dataset (SIBT1850; Walsh et al. (2015, updated 2016)). Prior to 1850, sea ice
188 extent and concentration are specified as the 1860–1891 HadISST2.3 climatology.

189 Thanks to international efforts facilitated by the Atmospheric Circulation Reconstructions over the Earth (ACRE)
190 initiative (Allan et al., 2011) and many volunteer efforts, there are millions more observations assimilated in 20CRv3
191 than in 20CRv2c. This represents an average of 5% more available observations per assimilation cycle in recent periods
192 (after about 1930), and up to 25% more available observations per cycle in earlier years. The new observational dataset,
193 the International Surface Pressure Databank (ISPD) version 4.7 (Cram et al., 2015; Compo et al., 2015), blends surface
194 and sea level pressure observations from the International Surface Database (ISD, (Lott et al., 2008; Smith et al., 2011))
195 with additional station observations, archived and previously undigitized terrestrial data submitted to the ISPD from
196 international ACRE partners, pressure reports for tropical cyclones from version V03r10 of the International Best
197 Track Archive for Climate Stewardship (IBTrACS, Knapp et al. (2010); Kruk et al. (2010) combined with additional
198 Pacific tropical cyclone data (Kubota, 2012), and marine observations from the International Comprehensive Ocean-
199 Atmosphere Data Set (Worley et al., 2005; Woodruff et al., 2011; Freeman et al., 2017) ICOADS3+ version 2. The latter
200 is our own improvement to ICOADS3 that includes recently-digitized and better positioned and quality-controlled
201 observations from ACRE-recovered expeditions, OldWeather.org, and the Australian Weather Detective project (see
202 (Spencer et al., 2019), <https://github.com/oldweather/ICOADS3.plus/releases> and Appendices A-B).

203 Unlike 20CRv2c, which used a 56-member ensemble Kalman filter with a digital filter applied to the background
204 forecast, 20CRv3 assimilates observations with an 80-member ensemble Kalman filter that utilizes a 4-dimensional
205 incremental analysis update (Bloom et al., 1996; Lei and Whitaker, 2016) and no digital filtering; see Section 3 and
206 Appendix A. Additionally, 20CRv2c interpolated station pressure observations to the model surface prior to assimilation,
207 while 20CRv3 uses the more typical procedure and assimilates them at the observation level, absorbing the vertical
208 interpolation of the background forecast into the observation operator (**H**). As will be discussed in Section 4, 20CRv3
209 includes a nonlinear quality control algorithm for the observations, an adaptive localization algorithm, an inflation
210 method based on relaxation-to-prior-spread, and an offline bias correction for marine observations prior to 1871
211 (see Appendices B-D for more details). 20CRv3 also includes an updated bias correction for station data over land:
212 these biases are 'learned' over a 60-day time period. That is, they are calculated as the average difference between the
213 observation and the first guess over the 60-day window (with a minimum of 31 days' worth of data in the window) prior
214 to the current assimilation step; if significant, these differences are subsequently removed from the observation at the
215 step prior to assimilation (see Compo et al. (2011), their Appendix B, for more details). Finally, the baseline observation
216 errors used in 20CRv3 are given in Table 1. Column 4 ('station') refers to observations of surface pressure, while column
217 5 ('SLP only') refers to stations that only reported pressure reduced to sea level. Observation errors are increased by
218 0.001 hPa per meter difference between the observation elevation and the model orography. These are the same errors
219 used in 20CRv2c, with the exception of tropical cyclone data (see Table A.1).

220 3 | ADDRESSING ISSUES IN 20CRV2C

221 The 20CRv3 dataset will build on two previous efforts: 20CRv2 and 20CRv2c. The 20CRv2 dataset represented an
222 important step forward for weather and climate research because it filled a need for a consistent, long-term, sub-daily

gridded atmospheric dataset using instrumental observations. As of the time of writing, the paper describing the 20CRv2 dataset (Compo et al., 2011) has more than 2000 citations (Google Scholar, accessed 4 Feb 2019). While useful, the 20CRv2 dataset has several issues, including a misspecification of polar sea ice that resulted in warm near-surface temperature biases (Brönnimann et al., 2012) and inhomogeneities associated with variations in observation density and its covariance inflation algorithm prior to 1952 (Ferguson and Villarini, 2012).

The 20CRv2c dataset was an effort to address those issues, use a novel SST specification, and include additional observations compared to 20CRv2. However, as more studies delved into different aspects of 20CRv2c, limitations of it became apparent. Simultaneously, the many studies using 20CRv2c motivated further data rescue efforts, and the amount of pressure observations available to be assimilated grew significantly, particularly in early years. Figure 1 illustrates the global annual average number of observations available to be assimilated in a 6-hour window of 20CRv2c (solid black) and 20CRv3 (dashed gray). Here, ‘available’ refers to observations that were rescued, digitized, externally quality controlled, and blended into the version of the ISPD used in the given reanalysis; it includes observations that may be flagged or thinned by the internal 20CR quality control system (see Section 4 and Appendix C for details.)

A new version of the 20CR system could make use of this growing set of observations, as well as general progress in modeling and data assimilation methods, and would provide a significantly improved dataset. Major issues in 20CRv2c, including inaccurate representations of uncertainty as well as large-scale biases and artifacts in sea level pressure, precipitation, and wind, also informed and motivated the development of the 20CRv3 system.

3.1 | Estimation of confidence

In order to make conclusions about the significance of trends, signals, and extrema from reanalyses, we must be able to quantitatively measure confidence in the datasets. A defining characteristic of 20CR is its use of an ensemble data assimilation method, which yields both a single best estimate of the analysis (the mean) as well as a quantification of the uncertainty around that estimate via the ensemble spread (the standard deviation). More spread implies more uncertainty, and less spread implies less uncertainty. In general, the uncertainty in the ensemble mean as an estimate will correlate negatively with the density of the available observational network. In addition, the variability of the ensemble mean in time, or temporal spread (Equation 1), can be used as an estimate of climatological uncertainty. At time t_k , the temporal spread of the ensemble mean over a window of length ΔT is given by:

$$\text{temp. spread}(t_k) = \left[\frac{1}{N_{time} - 1} \sum_{t=t_k-\Delta T/2}^{t_k+\Delta T/2} (x_{ensmean}(t) - \overline{x_{ensmean}})^2 \right]^{1/2}, \quad (1)$$

where N_{time} is the number of time steps in the window $[t_k - \Delta T/2, t_k + \Delta T/2]$, $x_{ensmean}(t)$ is the area-averaged ensemble mean of the variable of interest (for example, SLP) at time t , and $\overline{x_{ensmean}}$ is the time-average of the ensemble mean $x_{ensmean}(t)$ over the time window.

As an example, Figure 2 includes time series of uncertainty in sea level pressure over the zonal band from 65°S to 40°S calculated from 20CRv2c. This region is particularly important for investigations of anthropogenic CO₂ uptake, and long time series are needed for studies of its decadal variability (as discussed in, eg, Landschützer et al. (2015)). The analyzed sea level pressure ensemble spread is plotted (thick dark blue curve) along with the temporal spread of the analyzed sea level pressure ensemble mean (thin light blue curve) and the number of observations assimilated per 6-hour window (thin red curve, right hand axis) in this region. The temporal spread is calculated as the standard deviation of the ensemble mean across a centered time window using Eqn. 1 with $\Delta T = 61$ days, and all time series have a 1-year running average applied. This region has relatively few observations available (compare with Fig. 1), and the

effects of World War I (1914–1918) and World War II (1939–1945) are particularly striking (see shaded gray regions), as is the First GARP (Global Atmospheric Research Program) Global Experiment in 1979 (dashed line). The correlation r between the ensemble spread and the log of the number of observations assimilated per window is -0.96, demonstrating the strong inverse relationship between the ensemble spread and the observational network density.

However, ensemble spread is only an estimate of uncertainty, and it is not always reliable. For instance, a well-known issue with the EnKF is the tendency for ensembles to ‘over-tighten’ towards the mean, resulting in an ensemble spread that is overconfident and ultimately in filter divergence (that is, when the background ensemble standard deviation approaches 0 and the ensemble is unable to use information about observations) (Anderson and Anderson, 1999; Whitaker and Hamill, 2002). A common method to address this problem is ‘covariance inflation’; generally, this refers to artificially increasing the ensemble spread by, for example, applying a multiplicative factor greater than 1 to the ensemble covariance. When many observations are assimilated, the ensemble is more prone to collapse, and thus requires more inflation. In 20CRv2c, a simple multiplicative inflation factor (Anderson and Anderson, 1999) was applied to the ensemble covariance matrix at each step; this factor was predefined based on year and latitude. Table 2 shows the inflation parameters used in 20CRv2c. These time periods were chosen to loosely reflect availability and density of observations: for example, there were few National Meteorological Services organized prior to 1870, and thus the observational network was relatively sparse. The period 1871–1890 represents a transition period; with such developments as the founding of the International Meteorological Committee in 1873, the network of observations in the Northern Hemisphere becomes denser. Conversely, the Southern Hemisphere observation network remains relatively sparse into the 20th century.

While this method ensured that larger inflation parameters were applied when the observation network was more dense (e.g., in the Northern Hemisphere and in modern time periods), the abrupt changes in the parameters are responsible for artificial signals in the time series of uncertainty. The spike in ensemble spread in 1951 (solid black line in Fig. 2) is an artifact of the multiplicative inflation algorithm used in 20CRv2c: this is the year the inflation parameter in the Southern Hemisphere increased from 1.02 to 1.07 (Table 2), and there is no corresponding decrease in number of observations assimilated. In fact, 1951 marks an increase in assimilated SLP observations; this originally motivated increasing the inflation parameter in that particular year.

Another issue demonstrated by Fig. 2 is the under-confidence of the ensemble spread. As discussed earlier, the temporal spread can be used as a proxy for a climatological spread. Until the 1980s, the ensemble spread is larger than the temporal spread, suggesting that the ensemble was less confident than a climatological estimate. The inverse also occurs: the fixed inflation algorithm can result in too little inflation over data-rich regions, leading to overconfidence in these areas (not shown).

The version 3 system uses an improved inflation algorithm referred to as relaxation-to-prior-spread (Whitaker and Hamill, 2012). Using this algorithm, the inflation adapts to the observation network density. When there are few observations, the ensemble spread is hardly changed; when there are dense observations, the ensemble spread is ‘relaxed’ back to the prior spread, by an amount λ_{inf} . For every model grid point (x, y) and analysis time t , the inflation parameter λ_{inf} is given by:

$$\lambda_{inf}(x, y, t) = p_{relax} \left(\frac{\sigma_b(x, y, t) - \sigma_a(x, y, t)}{\sigma_a(x, y, t)} \right) + 1, \quad (2)$$

where $\sigma_b(x, y, t)$ is the standard deviation of the background ensemble, $\sigma_a(x, y, t)$ is the standard deviation of the analysis ensemble before inflation, and p_{relax} is a relaxation parameter that can vary from 0 (no inflation) to 1 (inflate to prior spread). The ratio of ensemble spread in Eqn. 2 implicitly depends on the density of the observation network in that region: a dense network will result in a smaller analysis ensemble spread, and thus a larger inflation parameter, and

vice versa. Initial tests with the 20CRv3 system used $p_{relax} = 0.9$ globally. These tests (not shown) suggested that this was too large in the Southern Hemisphere, as the uncertainty was larger than a climatological uncertainty. Thus, the final 20CRv3 system uses $p_{relax} = 0.9$ for $20^{\circ}\text{S}–90^{\circ}\text{N}$ and $p_{relax} = 0.7$ for $90^{\circ}\text{S}–30^{\circ}\text{S}$. In the transition zone $30^{\circ}\text{S}–20^{\circ}\text{S}$, p_{relax} varies linearly from 0.7 to 0.9. These values of p_{relax} do not change in time. Figure 3 shows representative examples of the adaptive inflation parameter λ_{inf} from four different years; a value of 1 is equivalent to no inflation.

The GFS model in 20CRv3 uses stochastic physics (Appendix A), which also contributes to the ensemble spread. This effect is particularly strong in the tropics, which reduces the need for inflation in this region (e.g., Fig. 3d). Outside of the tropics, the inflation factor depends on the observation network density: over the US and Europe, and throughout the Northern Hemisphere in recent years, the inflation factor is larger than elsewhere. Note also that the range of inflation parameter values used in 20CRv3 is much larger than was prescribed in 20CRv2c (compare Fig. 3 and Table 2).

Figure 4 illustrates the result of these changes in terms of the ‘confidence’ in fields of sea level pressure from versions 2c and 3 of 20CR during selected early 20th century boreal winters. Here, ‘confidence’ is defined as the difference of the normalized time-averaged ensemble standard deviation from 1:

$$conf = 1 - spread_{ens}/spread_{clim}, \quad (3)$$

where $spread_{ens}$ is the time-averaged standard deviation of the ensemble of analyzed SLP from the stated version of 20CR, and $spread_{clim}$ is the temporal standard deviation of the 20CRv2c ensemble mean 6-hourly SLP over Jan-Feb-Mar from 1981–2010. In other words, $spread_{clim}$ represents an estimate of the inherent weather variability; it is assumed to be time-invariant and independent of ensemble spread. Thus, a confidence value of zero (denoted by black contours in Fig. 4a-b) denotes ensemble spread identical to the climatological spread; greater confidence implies more certainty than climatology, and negative confidence implies less certainty than climatology. Aside from interannual variations in weather variability (e.g., Compo et al. (2001)), the minimum confidence value would be zero.

These maps demonstrate features of the new estimates of confidence in 20CRv3. In particular, there is more certainty over the high Arctic latitudes in version 3 (red shading in Fig. 4c in this region) than simply using a climatological mean as the analysis. There is also more spread over the densely-observed regions of North America and Europe (blue shading in Fig. 4c in these regions). Results (not shown) using independent observations from U.K. Daily Weather Reports comparing expected and actual errors suggest that this is an improvement, as the 20CRv2c analyses are overconfident over Europe in the 1900s. Similar overconfidence is found for 20CRv2c first-guess fields (not shown). We expect that the results would be similar for independent observations over North America. In contrast, the larger-than-climatological uncertainty over the high southern latitudes has been reduced but not eliminated, despite the decrease in p_{relax} discussed above. There is also a decrease in confidence in 20CRv3 throughout much of the tropics; this may be due to the stochastic physics described above. The decrease in confidence throughout the mid-latitude oceans suggest that further experiments with p_{relax} may be necessary in the future. While many of the differences are likely due to the new adaptive inflation algorithm, recall that 20CRv3 uses an 80 member ensemble, as opposed to the 56 members in 20CRv2c. The larger ensemble, as well as other updates to the 20CRv3 system, may also have contributed to greater consistency between the quantified confidence of version 3 and prior expectations.

3.2 | Global sea level pressure bias

Another significant issue in 20CRv2c, a sea level pressure bias prior to the 1870s, prevented this dataset from being as useful as it could have been for its full span. This bias is evident in globally-averaged time series of sea level pressure (Figure 5, blue curve) for most years prior to 1870. Relative to several reanalyses of varying timespans, including

ERA-Interim (orange), the historical reanalyses ERA-20C (green) and CERA-20C (gold), and a 56-member ensemble of simulations with the same version of the GFS used in 20CRv2c but without assimilation ('no DA'; red), the global SLP from 20CRv2c is as much as 2-4 hPa too low during the period of concern. Shading on Fig. 5 represents one standard deviation when ensemble estimates are available; note that the 20CRv2c spread in the biased period is still several hPa away from the 'no DA' mean and standard deviation.

The cause is revealed to be biased ship observations in the mid-19th century, first reported by Todd Mitchell at a marine data workshop (Diaz et al., 2002; Ansell et al., 2006; Allan and Ansell, 2006), combined with the 20CRv2c system allowing the global dry pressure to be updated during the assimilation cycle. The 20CRv2c system assimilated many low-biased ship observations throughout the world oceans. During the assimilation, the global SLP field and the global dry air pressure were updated to be lower and more consistent with these biased observations. This resulted in a feedback cycle, as the biased observations continued to be assimilated in the mid-19th century and the global SLP and dry air pressure fields continued to be lowered. While 20CRv2c included a bias correction to land stations, it did not include a marine observation bias correction algorithm. Figure 6a shows a map of the 1851–1853 time-averaged SLP anomaly fields from 20CRv2c analyses: note the widespread negative anomalies, particularly over the oceans. Panel (b) differs from (a) in that it used an experiment that assimilated about 10% fewer ship observations than 20CRv2c, but with an otherwise identical setup. Overall, the anomalies are less negative, demonstrating that assimilating more ship observations from 1851–1853 negatively biased the globally-averaged analyzed sea level pressure by as much as 4 hPa. Note that these ships were not chosen on an a priori basis: this illustrates the strong effect of a small number of biased observing platforms within a cycled data assimilation system.

Two improvements in 20CRv3 will address this issue. First, the global dry pressure can no longer be updated within the assimilation: instead, it is specified at 98.3050 kPa (Trenberth and Smith, 2005). This prevents the feedback loop with the biased ship observations that allowed the global sea level pressure bias to persist for nearly two decades of 20CRv2c data. Second, to directly address the observation bias, a correction is applied to marine observations prior to 1870. Investigations into the individual observations found that the negative bias is not consistent across different voyages in this time period, suggesting that a single bias correction for all marine observations in this time period would not be sufficient. Thus, a bias for each individual ship is calculated as the mean deviation from the 20CRv2c 1981–2010 climatology, and subtracted from the marine observations prior to assimilation (see Appendix B for more details).

Figure 7 illustrates a test of these new procedures. Fig. 7a shows the 20CRv2c SLP annual anomaly for 1854; note the consistently negative differences throughout the tropics and midlatitudes. The effect of constraining dry pressure in the version 3 system without bias correcting the observations is shown in Figure 7b. There are still negative anomalies in the highly-trafficked regions of the ocean (around Cape Horn, South America; the North Pacific Ocean off the coast of the US; and the North Atlantic Ocean). In order to retain the fixed dry pressure, this leads to an increased SLP anomaly where there are fewer observations, particularly around the poles. Figure 7c includes both the fixed dry pressure and the bias-corrected ship observations. The negative anomalies in high-density marine regions are now almost entirely removed, and while the positive anomaly over the high southern latitudes remains, it has been diminished. The black curves in Fig. 5 represent the annual global SLP from 20CRv3 during three test periods, and demonstrate the large-scale effects of these changes to the 20CRv3 system.

As with many bias correction schemes, it is possible that this method is removing real signals from historical observations by forcing them towards a modern climatology. For example, the negative SLP anomalies in the southern midlatitudes prior to bias correction (Fig. 7b) are assumed to be effects of biased observations from ships, as these anomalies are strongest in heavily-trafficked shipping lanes and whaling areas. However, this pattern could be a real climatological shift in wave number 3 of the zonal flow in the Southern Hemisphere (see, for example, van Loon and Jenne (1972); Raphael (2004)) and would be erroneously removed by the bias correction scheme (Fig. 7c). Nevertheless,

in the absence of more information about these pressure observations or independent reconstructions of the mid-19th century SLP fields for validation, this procedure provides an improvement over uncorrected marine observations leading to spurious SLP trends (e.g., Fig. 5). Deeper investigations into the cause of this observational bias (such as changes in meteorological logs or barometer-correction practices over the period 1850-1860) could allow for more realistic bias correction schemes in the future.

3.3 | Artifacts in precipitation and wind

While the global SLP trend prior to 1870 in Figure 5 could be attributed in some way to the observations, other artifacts can be traced back to the assimilation method. One example stems from the use of a digital filter (Lynch and Huang, 1992; Huang and Lynch, 1993) in the forecast step of 20CRv2c that was implemented to temporally smooth the physical fields after the EnKF update (Appendix A). Without this filtering, imbalances introduced by the EnKF update would have resulted in numerical noise during the forecast step, which in turn would have contaminated the forecasts and the covariance estimate during the next assimilation step, degrading the accuracy of the analysis. The digital filter was active for forecast hours 0-3, and was turned off for hours 3-6. One effect of the digital filter switching on and off is an artificial positive trend in the tendency of precipitation rates from consecutive forecast windows (Figure 8a).

Instead of a digital filter, the version 3 system uses a 4D incremental analysis update (4DIAU) (Bloom et al., 1996; Lei and Whitaker, 2016) to mitigate the imbalances introduced by the EnKF update. Essentially, the updates calculated by the EnKF analysis step are applied as a model forcing at every time step within the forecast, preventing gravity wave noise from contaminating its short-term evolution. Unlike the digital filter, the temporal smoothing in the 4DIAU is effectively only applied to analysis increments, not to the fields output from the model, thereby eliminating the spurious tendency trends seen during the forecasts of version 2c. Figure 8b demonstrates the improvement over the digital filter: the precipitation rate biases have almost entirely disappeared. Note that the spatial average of the tendencies (difference between 3-6 hour and 0-3 hour forecasted precipitation rates) from 20CRv2c fields (Fig. 8a) is 0.72 mm/day, while the average from 20CRv3 (Fig. 8b) is 0.05 mm/day. These figures show the annual average for 2002 but are representative of all available years.

Despite this change, the global annual average precipitation rate in tests with the 20CRv3 system is nearly the same as 20CRv2c. Figure 9 shows the 2002 annual average precipitation rates for (a) 20CRv2c, (b) 20CRv3, and (c) the gridded, blended satellite/gauge precipitation dataset from NASA's Global Precipitation Climatology Project (GPCP; Adler et al. (2003)). The 20CRv3 field has a stronger separation in the western tropical rainband than 20CRv2c, leading to a double Inter-Tropical Convergence Zone (ITCZ) that is not as apparent in the GPCP dataset. Note that both versions of 20CR also overestimate global precipitation rates relative to GPCP; investigations into this issue are ongoing.

Figures 8a and 9a show another artifact of 20CRv2c, previously identified by Kent et al. (2013): namely, a spectral ringing characteristic in the precipitation mean and difference fields. This artifact is even more apparent in the 10m wind fields (Figure 10a). This effect is the result of an error in the spectral transform of a higher-resolution orography to the lower-resolution field used as an input to 20CRv2c (Fig. 10c). Since 20CRv3 uses a model at a higher resolution than 20CRv2c, it does not suffer from this issue as dramatically (Fig. 10b & d), and the precipitation and wind fields lack any spectral ringing signals.

4 | ADDITIONAL IMPROVEMENTS IN 20CRV3

In addition to the specific developments in the version 3 system that were designed to ameliorate issues in 20CRv2c, early tests with the 20CRv3 system suggest that it will benefit from other updates to the system leading to overall improvements. In particular, the version 3 system uses adaptive quality control and localization and specifies smaller tropical cyclone observation errors. These changes, in conjunction with a newer, higher-resolution forecast model, a larger observational database, and the improvements described in Section 3, yield results suggesting that 20CRv3 will have smaller forecast errors, large-scale reductions in model bias, and more accurate representations of hurricanes.

4.1 | Adaptive methods for assimilating observations

All versions of 20CR use an ensemble Kalman filter to assimilate observations. It is well-known that localization is required to prevent spurious ensemble cross-correlations from developing far away from the assimilated observations (Houtekamer and Mitchell, 1998, 2001; Hamill et al., 2001; Anderson, 2007). The use of localization in ensemble data assimilation systems for weather prediction is crucial, since current-generation systems are being run with ensemble sizes many orders of magnitude smaller than the size of the forecast model state vector. Traditional localization schemes use a smooth cutoff function, such as the piecewise continuous fifth-order polynomial function described by Gaspari and Cohn (1999), to taper the covariances to zero at a given distance away from an observation. Typically, this 'Gaspari-Cohn' localization is a function of only the horizontal distance between an observation and a state variable, and is described by a single parameter that is related to the distance at which the Gaspari-Cohn function goes to zero. The optimal value for the localization length scale may be a function of many aspects of the data assimilation system, such as the density of the observing system and the scale of the phenomena being observed. This makes tuning the localization length scale difficult, especially when the observing system is very inhomogeneous, and many different scales are being observed simultaneously. The 20CRv2c system used a localization radius of 4000 km for all times and locations based on early tests (Whitaker et al., 2004); a relatively large value was chosen to maximize the use of observations in data-sparse regions and to minimize the generation of small-scale noise by the EnKF update. In addition, a five-step quality control (QC) process was employed in 20CRv2c; this is the same process used in 20CRv2 and described in Appendix B of Compo et al. (2011).

Since the 20CR system only assimilates surface pressure observations and the network can become quite sparse in the 19th century, it is important to extract the most information from each observation. In order to make better use of the observations, 20CRv3 uses an adaptive quality control procedure jointly with an adaptive localization algorithm. Observations must pass two initial gross QC steps: if the observation is outside a plausible range or if the observation is too far from the first guess, the observation is rejected. The first step will reject an observation that is outside the range 850 and 1090 hPa. The second step will reject an observation x_{ob} if it is too far from the first guess x_{fg} :

$$|x_{ob} - x_{fg}| > 3.2 * \sqrt{\sigma_b^2 + \sigma_{ob}^2}, \quad (4)$$

where σ_b^2 is the variance of the first guess ensemble interpolated to the observation time and location and σ_{ob}^2 is the observation error variance. Unlike 20CRv2c, version 3 does not utilize a 'buddy check' or a thinning algorithm to reject observations that degrade the fit of the analysis to nearby observations or that do not decrease the analysis ensemble spread. Instead, the adaptive quality control assigns these observations larger errors and smaller localization radii, so that their region of influence is essentially zero. Details of the adaptive quality control and localization procedures used in 20CRv3 can be found in Appendices C-D.

Figure 11 shows maps of observations within a single assimilation window for four test years: 1854, 1915, 1935, and 2000. Note that, as the observation network becomes denser, the localization lengths generally decrease. In 1854 and 1915, the observation network is relatively sparse, and most observations have localization length scales near the maximum allowed of 4000 km. In the year 2000, however, most observations located within densely observed areas have localization length scales closer to 1000 km, though there are a few observations within these areas that the algorithm selects for longer localization length scales. Observations located within areas that are sparsely observed (such as the Southern Ocean and Antarctica) still have fairly long localization length scales in the year 2000. This new procedure allows many more observations to be assimilated within 20CRv3 while adaptively allowing observations with significant beneficial effects to have larger ranges of impact, and observations that have less beneficial effects to have smaller ranges.

4.2 | Observation statistics

Observations have a large impact on overall performance of reanalyses: inaccurate observations as well as the incorrect prescription of their errors can impact global fields and their trends (recall the global SLP bias in Figure 5). It is crucial, then, to investigate the behavior of their statistics in the context of the full system. Here we show that, while 20CRv2c performs fairly well under many measures, the updated algorithms used in 20CRv3 produce clear improvements in several test periods.

Statistics of the departures of observations from the first-guess field can provide one measure of how well the entire system is performing, particularly when compared with statistics of the expected errors. The 'actual' error is defined as:

$$\text{RMSE}_{\text{actual}} = \left[\frac{1}{N_{\text{obs}}} \sum_{i=1}^{N_{\text{obs}}} (x_{\text{ob},i} - x_{\text{b},i})^2 \right]^{1/2}, \quad (5)$$

where i indexes all N_{obs} observations that are contributing to the statistic (in space or time), $x_{\text{ob},i}$ is the i^{th} observation, and $x_{\text{b},i}$ is the first-guess field interpolated to the i^{th} observation time and location. The expected error is then defined as:

$$\text{RMSE}_{\text{exp.}} = \left[\frac{1}{N_{\text{obs}}} \sum_{i=1}^{N_{\text{obs}}} (\sigma_{\text{ob},i}^2 + \sigma_{\text{b},i}^2) \right]^{1/2}, \quad (6)$$

where i indexes the same N_{obs} observations as above, $\sigma_{\text{ob},i}^2$ is the i^{th} observation error variance, and $\sigma_{\text{b},i}^2$ is the variance of the first guess ensemble, interpolated to the i^{th} observation time and location. As shown by Desroziers et al. (2005), under the assumptions that the observation and background errors are uncorrelated and unbiased, these errors should be equivalent. In a DA system that is performing well, the actual errors should not be larger than the expected errors. We consider time series of regionally- and annually-averaged surface pressure forecast errors for the Northern Hemisphere (20°N to 90°N), tropics (20°S to 20°N), and Southern Hemisphere (90°S to 20°S). That is, the statistics in Equations 5-6 are calculated using all observations in the given region for each year. These are plotted in Figure 12 for 20CRv2c (blue) for all years and 20CRv3 (black) for three test periods.

As expected from EnKF theory and seen with 20CRv2 (Compo et al., 2011), errors decrease in time as observations are denser and more accurate. Note that this is not a result of any 'tuning'. The Southern Hemisphere errors from 20CRv2c match the expected errors particularly well in all decades after 1860. The 20CRv2c errors in the tropics are

487 less consistent, and the actual errors in the Northern Hemisphere are almost always larger than the expected errors,
488 by over 1 hPa in earlier decades and by 0.3-0.5 hPa in recent decades. This suggests that, in the 20CRv2c system, the
489 errors assigned to observations might be too low, the first guess ensemble spread is too small, the observations or first
490 guess fields are biased, or a combination of these.

491 The preliminary 20CRv3 errors (black curves in Fig. 12) show improvements in nearly every test period. While the
492 actual errors in the 1851 – 1870 test period are still larger than the expected errors, this discrepancy is smaller than
493 in 20CRv2c. Recall from Section 3 that, prior to 1871, a bias correction was made to marine observations in 20CRv3,
494 in addition to the station observation bias correction. Although dry air mass conservation is mainly responsible for
495 removing the low-pressure bias (Fig. 7), the ship bias correction provides further improvement. For the modern period
496 in all regions, the actual error is always less than expected. This suggests that the assigned observation errors may
497 be too large for modern years, and future work may investigate the effects of time-varying observation errors as in
498 Laloyaux et al. (2018). Nevertheless, the overall effect of the new algorithms in the version 3 system, including ship bias
499 correction, is to decrease the RMS errors in several different test periods.

500 These improvements in RMS errors may be due to the updated model, as well as to the new algorithms implemented
501 in the 20CRv3 system. This is supported by investigations into the station bias corrections: recall that these corrections
502 are based on 60-day average differences between observations from each station and the first-guess pressure at that
503 location. Ideally, the consistent mismatch between observations and the model first guess are biases in the observations
504 that are removed; however, the mismatch could be due to model errors, and the algorithm would actually be adjusting
505 the observations away from reality and towards the biased model state. In particular, it is likely that biases with large-
506 scale spatial patterns are model errors, though they could result from national issues producing similar biases (Slonosky
507 and Graham, 2005) or international changes in observing practices that are adopted by nations at different rates (see
508 discussion in Trenberth and Paolino (1980)). Conversely, small-scale biases may point to a mis-assignment of station
509 elevation or position: these are observational biases that should be corrected.

510 Figure 13 (left column) shows the annual average station pressure biases from 1960, 1980, and 2000 that were
511 removed from observations in 20CRv2c. Note the annual values in the region over eastern Europe and much of northern
512 Asia are consistently negative, suggesting a model bias (see also van den Besselaar et al. (2011)). Conversely, the version
513 3 data does not show the same spatial or temporal consistency of negative values in this region (Fig. 13, right column).
514 This suggests that the model used in version 3 may be less biased than in 20CRv2c. Another cause could be due to the
515 process of the station bias correction: 20CRv2c calculated biases from the observations interpolated to the model
516 surface, but inadvertently applied the correction at the level of the observation; in 20CRv3, the bias correction is
517 calculated and applied at the level of the observation.

518 Unlike the Eurasian biases, consistent regional biases over the US have hardly changed in 20CRv3; it is unclear
519 whether this is a model bias effect or not. Other possible causes of large-scale biases include orography (biases over
520 mountain ranges tend to be consistent; see the Himalaya) and nationality (due to country-specific calibration and
521 correction methods; c.f. the Canadian ‘50-foot rule’ (Slonosky and Graham, 2005)). Finally, version 3 includes many
522 other changes to the assimilation method and the observation handling, as well as changes to the forecast model, so
523 it is difficult to confidently conclude that the negative bias over northern Asia was a model error that has been fixed.
524 Regardless, the overall mismatch between station observations and first-guess fields has been notably diminished in
525 20CRv3. This leads to analyzed SLP fields (Figure 14) and 500 hPa geopotential height fields (Figure 15) that are closer
526 to those of ERA-Interim and JRA-55, particularly in northern Eurasia.

4.3 | Representation of hurricanes

Historical reanalyses are especially useful for studying extreme weather events, since these are by definition rare but high-impact events. Tropical and extratropical cyclones are of particular interest as they can result in loss of life and enormous financial costs. To improve understanding and predictions of these storms, it is necessary to improve our understanding of the large-scale drivers of them as well as how storm characteristics are changing as the climate changes. If historical reanalyses can accurately capture these storms, they provide a long, consistent sample of such extreme events and their associate large-scale environment.

In order to represent tropical cyclones (TCs), 20CRv2c assimilated TC data from IBTrACS (Knapp et al., 2010) in addition to land station and marine pressure observations. IBTrACS consists of actual pressure measurements, pressure reports calculated as time-interpolated values from tropical cyclone warning centers, and wind-derived central pressure reports; see Compo et al. (2011); Knapp et al. (2010) for more details. Since these data are often significantly lower pressure values than the nearby station observations, they would generally fail the quality control step that compares observations to their nearest neighbors (see Appendix B of Compo et al. (2011)); therefore, the 20CR system has IBTrACS data bypass these checks and assimilates these deep-low data.

In version 2c, these data were assigned observation errors that were much higher than for any other type of observation to prevent numerical instabilities from arising immediately after assimilation; see Table A.1. Despite digital filtering to smooth the evolution of the post-update fields, tests using smaller errors would occasionally still generate amplifying gravity waves and numerical instability. While the large error assignment eliminated this problem, the resulting 20CRv2c analyses can have central pressure values that are much higher than the IBTrACS data, sometimes by 40 hPa or more. The version 3 system, with an updated, higher-resolution forecast model and 4DIAU, can use these observations more effectively. Assimilating TC low-pressure values into the version 3 system does not generate instabilities, and so the IBTrACS data can be assigned smaller observation errors (see Table 1). This often yields stronger cyclones with central pressure analyses that are closer to the original IBTrACS value.

As an example, we investigate a strong hurricane that hit Galveston, Texas in August 1915. Figure 16 illustrates the analyzed sea level pressure fields (contours) from 4 reanalyses, as well as locations of observations available to each system between 16 Aug 1915 2100 UTC and 17 Aug 1915 0900 UTC (circles); this window was chosen so that observations assimilated at 0000 UTC would be shown as well as those assimilated at 0600 UTC. For each system, observations that were assimilated are shown as solid circles, while observations that were rejected by the system's quality control step are open circles. Blue circles represent station and marine observations, and red circles represent IBTrACS data. 20CRv2c (Fig. 16a) assimilated the IBTrACS report of 940 hPa on 17 Aug 1915 at 0600 UTC, producing an analyzed value of 986 hPa at the center of the storm. In version 3 (Fig. 16b), the storm is even stronger, and the analyzed value at the center of the storm has decreased to 962 hPa, reducing the observation-analysis departure calculated from 20CRv2c by half. Since the IBTrACS reports were available and assimilated into 20CRv2c and 20CRv3 beginning on 1 August 1915, this hurricane evolved and strengthened continuously in time in both versions of 20CR (not shown.) For comparison, the ERA-20C quality control rejected the IBTrACS observations (Fig. 16c) and analyzed a low pressure system that is weaker than that of 20CRv2c and has a misaligned center. The CERA-20C system also rejected the IBTrACS observations, but additionally assigned larger errors to the nearby station data than ERA-20C (Laloyaux et al., 2018), thereby showing no trace of the storm (Fig. 16d). Laloyaux et al. (2018) conducted experiments with the CERA-20C system in which this type of observation was white-listed, and found this yielded better performance than CERA-20C for two hurricanes in 1900 and 2005 (their Fig. 5).

5 | REMAINING ISSUES

While the changes from the version 2c system to the version 3 system have resulted in many improvements across the board, there are several remaining issues in 20CRv3 as well as new questions that have arisen. For instance, recall (Figure 9) the precipitation biases that have strengthened in 20CRv3, particularly the appearance of a double ITCZ and the overestimation of global precipitation rates relative to GPCP. The Southern Hemisphere confidence fields (Figure 4) also demonstrate that there is some remaining large uncertainty over Antarctica (though these areas are relatively small), despite tests that led to adjusting the inflation parameter in the Southern Hemisphere.

Figure 7 and Figure 14a-b demonstrate another potential issue with the Southern Hemisphere: a high pressure bias over Antarctica. Figure 7 shows that the 1854 annual average sea level pressure over Antarctica in 20CRv3 is several hPa higher than the 20CRv2c modern climatology, and this anomaly is larger in 20CRv3 than it was in 20CRv2c. Figure 14 demonstrates that 20CRv3 also displays this high pressure bias in a modern difference calculated with respect to ERA-Interim. However, the strong difference relative to ERA-Interim is mainly over the Antarctic landmass, which has a fairly high topography, so the sea level pressure field is likely not an appropriate variable to consider when diagnosing the mass or circulation field of this region. Indeed, the SLP difference with JRA-55 (Fig. 14c-d) has the opposite sign in this region.

A third Southern Hemisphere issue, regarding a trend in sub-Antarctic sea level pressure, was first brought to light during an investigation of ERA-20C (Poli et al., 2015, 2016) and is demonstrated in Figure 17. This figure shows the seasonal time series of sea level pressure area-averaged poleward of 60°S for 20CRv2c (blue), ERA-20C (green), CERA-20C (gold), and ERA-Interim (orange), as well as data from an ensemble of model simulations using the 20CRv2c system but that did not assimilate any observations ('no DA', red) and preliminary 20CRv3 data for the test periods 1851-1870, 1910-1930, and 1990-2010 (black). ERA-20C has a high pressure bias south of 60°S in the early 20th century that is particularly strong in austral summer (green curve in Fig. 17a between 1900 and 1930). Comparisons with 20CRv2c show that it has a similar bias as ERA-20C in other seasons, but a weaker bias than ERA-20C in Dec-Jan-Feb. There is a drop and subsequent increase in SLP from 20CRv2c in all seasons (most notably in Sept-Oct-Nov) from 1890-1910, with another significant drop-off between 1940 and 1960. The preliminary 20CRv3 data agrees with the 20CRv2c data for the most part, though the early 20th century March-April-May SLP has been diminished. In all seasons, though, the modern 20CRv3 SLP is still about 5 hPa lower than the early 20th century SLP.

ERA-20C and the 20CR datasets used entirely different models and assimilation methods but show similar trends, which suggests the culprit is in the observations. Poli et al. (2015) and Laloyaux et al. (2018) assert that the problem was caused not by a bias in the observations, but by the spatial pattern of observations at this time in the Southern Hemisphere. In particular, most of the observations are located in the subtropical high-pressure belt; the positive increments from assimilating these observations were communicated to the unobserved, and thus unconstrained, region farther south. They argue that this is caused by observation errors that are too small in ERA-20C; thus in CERA-20C, larger observation errors were assigned in this time period. This has significantly decreased the trend in SLP from CERA-20C in all seasons (gold curves in Fig. 17), though it remains somewhat in DJF, when the bias in ERA-20C was most obvious. Hegerl et al. (2018) point out the HadCRUT4 temperature dataset (Morice et al., 2012) also exhibits anomalously cold SSTs during the years 1906-1915 in the Southern Ocean (their Fig. 2c), possibly due to instrumental biases or uncertainties in the sea ice fields; investigations into this issue and possible connections with the SLP signals in Fig. 17 are ongoing.

6 | CONCLUSIONS

With the growing need to understand and predict climate and extreme weather variations on decadal to centennial timescales, the use of historical reanalyses continues to expand in areas such as assessments of long-term climate change, investigations of extreme events, and detailed histories of weather. It is, therefore, becoming more important that these reanalyses be reliable, both in their state estimates and their quantification of uncertainty. Users must recognize when and where historical reanalyses can be confidently utilized, and when caution should be taken (or a different dataset chosen). This work seeks to illuminate particular aspects of 20CRv2c that require careful consideration, the ways in which these issues informed the development of the 20CRv3 system, and particular aspects of 20CRv3 that show preliminary improvements over 20CRv2c.

The Twentieth Century Reanalysis version 2c improved upon several issues discovered in the previous NOAA-CIRES historical reanalysis, 20CRv2, but other problems remained. They provided specific focus areas when developing the NOAA-CIRES-DOE 20CRv3 system. Indeed, many of the issues in 20CRv2c discussed here have been ameliorated in 20CRv3 due to a combination of factors: a newer NCEP GFS forecast model with higher resolution; improved data assimilation algorithms, observation processing, and quality control; and an updated ISPD observation database. Several other issues with 20CRv2c exist that have not been discussed here, including spinup effects in sea ice thickness, snow depth, and soil moisture, and biases in the upper-stratospheric temperatures; some of these issues are reduced in 20CRv3 and will be discussed in future work.

Preliminary results with the 20CRv3 dataset are quite promising, though they are already highlighting areas for future research, particularly in the 'Deep South' of the Southern Hemisphere. The confidence in that region remains too low; further work regarding the relaxation-to-prior-spread inflation algorithm in this region may be necessary to increase the confidence to more realistic values. A larger set of available observations in this region would also increase the confidence (recall Figure 2), motivating greater data rescue efforts here. Gathering high-quality observations in these sparsely-observed regions remains a challenge within the data rescue community (Allan et al., 2011; Brönnimann et al., 2018), but new data rescue efforts (SouthernWeatherDiscovery.org) are beginning to address this. More data are also needed in other sparsely-observed regions, as well as globally in the early 19th century. Other data rescue efforts (including ACRE activities, WeatherRescue.org, the Copernicus Climate Change Service South America data rescue project, and the UK/China Climate Science for Service Partnership) have the potential to significantly add to the observational database in these regions.

Despite some remaining challenges with 20CRv3, there are early suggestions that this dataset will be useful for studies in which 20CRv2c required more cautious analysis: for example, tropical cyclones seem to show much stronger signals in 20CRv3 than in 20CRv2c. This suggests that 20CRv3 may be used for validating ongoing historical tropical cyclone research that extends IBTrACS back in time (Diamond et al., 2012), and for corroborating partial or discontinuous storm track information (e.g. when storm systems passed close to islands or ships.) Utilizing an updated inflation algorithm also allows for more consistent studies of long-term trends and uncertainty, where 20CRv2c exhibited artificial signals due to abrupt parameter changes.

Since the process of creating historical reanalyses is a continuous cycle of improvement, we are already looking ahead to further upgrades to the 20CR system. In particular, NCEP has recently significantly updated their global forecast system with a finite volume, cubed sphere model (Harris and Lin, 2013) (preliminary documentation available at <https://vlab.ncep.noaa.gov/web/fv3gfs/>); the changes resulting from this model versus the previous spectral model need to be investigated. Recent investigations into coupled data assimilation algorithms, and the first implementation of a quasi-strongly coupled data assimilation algorithm in CERA-20C (Laloyaux et al., 2018), suggest that future versions of 20CR could benefit from coupled systems. Finally, while all versions of 20CR so far have only assimilated surface

648 pressure, the possibility of assimilating other types of data (such as marine winds, sea ice observations, or precipitation)
649 seems to be more feasible as data assimilation algorithms continue to mature.

650 ACKNOWLEDGEMENTS

651 Support for the Twentieth Century Reanalysis Project is provided by the Physical Sciences Division of the NOAA Earth
652 System Research Laboratory, the US Department of Energy, Office of Science, Office of Biological and Environmental
653 Research (BER), and by the National Oceanic and Atmospheric Administration (NOAA) Climate Program Office. This
654 research used resources of the National Energy Research Scientific Computing Center (NERSC), a U.S. Department of
655 Energy Office of Science User Facility operated under Contract No. DE-AC02-05CH11231. Some computing was also
656 performed on NOAA's Remotely Deployed High Performance Computing Systems.

657 P. Brohan's (UK Met Office) extensive work on ICOADS and on the marine bias correction algorithm used in 20CRv3
658 is gratefully acknowledged. M. Benoy for the Citizen Science Unit of the Australian Meteorological Association, working
659 with the Australian Bureau of Meteorology, is gratefully acknowledged for ongoing support. Collaborations with N.
660 Rayner and the UK Met Office in the development, production, and use of HadISST boundary conditions are gratefully
661 acknowledged. H. Maechel's (DWD) contribution of German climate observations is gratefully acknowledged. The
662 authors would like to acknowledge the consultants of NERSC for their help with implementing the 20CRv3 system.
663 The authors would also like to thank the following individuals for their invaluable contributions of observations to the
664 ISPD: L. Alexander (Univ. of New South Wales), M. Barriendos (Univ. of Barcelona), T. Brandsma (KNMI), Y. Brugnara
665 (Univ. of Bern), O. Bulygina (All-Russia Research Institute of Hydrometeorological Information), A. Dawson (Univ.
666 of Aberdeen), J. Filipiak (Univ. of Gdansk), P. Groisman (NC State University Research Scholar at NOAA NCEI), J.
667 Holopainen (Univ. of Helsinki), D. Jones (Australian Bureau of Meteorology), T. Jónsson (Icelandic Met Office), J. A.
668 López (Instituto Nacional de Meteorología, Madrid), O. Mestre (Météo-France), A. Moberg (Stockholm University),
669 O. Nordli (Norwegian Meteorological Institute), M. Rodwell (ECMWF), T. Schmith (Danish Meteorological Institute),
670 L. Srncic (Croatian Meteorological and Hydrological Service), M. Tolstykh (Hydrometcentre of Russia), N. Westcott
671 (Midwestern Regional Climate Center), and P. Woodworth (National Oceanography Centre). IBTrACS data are courtesy
672 of K. Knapp (NOAA/NCEI). P. Lalouaux (ECMWF) is thanked for discussions regarding tropical cyclone representation.
673 The efforts of the NCAR Data Engineering and Curation Section, especially D. Schuster, R. Conroy, and C.-F. Shih are
674 acknowledged. The technical support of the IT group of the NOAA Earth System Research Laboratory Physical Sciences
675 Division is acknowledged. Partial support from SwissRe and collaboration with P. Zimmerli is acknowledged. Comments
676 from A. Shlyaeva (CIRES/NOAA) on an earlier version improved this manuscript.

677 J. Kennedy was supported by the Met Office Hadley Centre Climate Programme funded by BEIS and Defra. M.
678 Brunet acknowledges Copernicus Climate Change Service (C3S)/ Data Rescue Service (DRS) (Contract code: ATT
679 3670; FENIX: T17088S). J. Gergis was funded by Australian Research Council Project DE130100668. E. Hawkins was
680 supported by the UK National Centre for Atmosphere Science. A. Kaplan acknowledges the 2002 grant from the LDEO
681 Climate Center and NOAA awards NA03OAR4320179 and NA17OAR4310156. The research work of R. Przybylak
682 and P. Wyszynski was supported by the National Science Centre, Poland (Grants No. DEC-2012/07/B/ST10/04002
683 and 2015/19/B/ST10/02933). M. A. Valente acknowledges Instituto Dom Luiz - Faculty of Science of the University
684 of Lisbon, Instituto Português do Mar e da Atmosfera (IPMA), Instituto Geofísico do Porto, Instituto Geofísico da
685 Universidade de Coimbra, Projects SIGN (FCT-POCTI), ERA-CLIM (FP7) and ERA-CLIM2 (FP7).

686 The Justus Liebig University of Giessen, Germany is thanked for financial support to digitise, quality control and
687 analyse early instrumental meteorological data across the world. The following people are financially supported by the
688 University of Giessen and digitized subdaily pressure data: L. Dergianli, G. Kelly, D. Xoplaki, V. Iakovoglou, E. Kaimasidou,

689 E. Tsalkitzidou, M. Athanasiou, L. Feger, A. Megalou, C. Chandolia, E. Fleitmann, P. Zafeiropoulou, K. Nan, M. Ostheimer,
690 J. Schermuly, C. Mett, L. Theile, J. Zuckermann, P. Strehlau, C. Samaras, A. Tsikerdakis, C. Athanasiou, J. Braun, T. Sperzel,
691 J. Damster, N. Luther, M. Miltscheff-Petroff, M. Kelbling, Griechbaum, M. Hänsgen and J. Viezens. L. Dergianli is
692 acknowledged for quality control, coordination, management and preparation of all Uni Giessen data. S. Jourdain,
693 M. A. Valente, M. Brunet, J. Luterbacher, R. Allan, G. P. Compo, P. Jones, S. Brönnimann, and A. Lorrey acknowledge
694 Package 3 of the Copernicus Climate Change Service 311a Lot1 for Collection and Processing of In Situ Observations
695 Data Rescue. J. Luterbacher and R. Allan acknowledge Climate Science for Service Partnership China Project (CSSP).
696 J. Luterbacher also acknowledges the DAAD project 'The Mediterranean Hot-Spot' and the JPI-Climate/Belmont
697 Forum collaborative Research Action 'INTEGRATE, An integrated data-model study of interactions between tropical
698 monsoons and extratropical climate variability and extremes'. S. Brönnimann additionally acknowledges funding from
699 the European Research Council under H2020 (Grant PALAEO-RA, 787574).

700 GPCP data provided by the NOAA/OAR/ESRL PSD, Boulder, Colorado, USA, from their web site at
701 <https://www.esrl.noaa.gov/psd/>. The ERA-Interim, ERA-20C, and CERA-20C datasets are courtesy of ECMWF. The
702 scientific results and conclusions, as well as any views of opinions expressed herein, are those of the authors and do
703 not necessarily reflect the views of the University of Colorado, NOAA, the Department of Commerce, or any other
704 organization associated with this work.

705 REFERENCES

- 706 Adler, R., Huffman, G., Chang, A., Ferraro, R., Xie, P., Janowiak, J., Rudolf, B., Schneider, U., Curtis, S., Bolvin, D., Gruber, A.,
707 Susskind, J. and Arkin, P. (2003) The version 2 Global Precipitation Climatology Project (GPCP) monthly precipitation anal-
708 ysis (1979-present). *J. Hydrometeor.*, **4**, 1147–1167.
- 709 Allan, R. and Ansell, T. (2006) A new globally complete monthly historical gridded mean sea level pressure dataset (HadSLP2):
710 1850–2004. *Journal of Climate*, **19**, 5816–5842. URL: <https://doi.org/10.1175/JCLI3937.1>.
- 711 Allan, R., Brohan, P., Compo, G. P., Stone, R., Luterbacher, J. and Brönnimann, S. (2011) The International Atmospheric Circulation
712 Reconstructions over the Earth (ACRE) initiative. *Bulletin of the American Meteorological Society*, **92**, 1421–1425. URL:
713 <https://doi.org/10.1175/2011BAMS3218.1>.
- 714 Anderson, J. L. (2007) Exploring the need for localization in ensemble data assimilation using a hierarchical ensemble fil-
715 ter. *Physica D: Nonlinear Phenomena*, **230**, 99 – 111. URL: <http://www.sciencedirect.com/science/article/pii/S0167278906002168>. Data Assimilation.
- 717 Anderson, J. L. and Anderson, S. L. (1999) A Monte Carlo implementation of the nonlinear filtering problem to produce ensem-
718 ble assimilations and forecasts. *Monthly Weather Review*, **127**, 2741–2758.
- 719 Ansell, T. J., Jones, P. D., Allan, R. J., Lister, D., Parker, D. E., Brunet, M., Moberg, A., Jacobeit, J., Brohan, P., Rayner, N. A., Aguilar,
720 E., Alexandersson, H., Barriendos, M., Brandsma, T., Cox, N. J., Della-Marta, P. M., Drebs, A., Founda, D., Gerstengarbe, F.,
721 Hickey, K., Jónsson, T., Luterbacher, J., Nordli, Ø., Oesterle, H., Petrakis, M., Philipp, A., Rodwell, M. J., Saladie, O., Sigro, J.,
722 Slonosky, V., Srnec, L., Swail, V., García-Suárez, A. M., Tuomenvirta, H., Wang, X., Wanner, H., Werner, P., Wheeler, D. and
723 Xoplaki, E. (2006) Daily mean sea level pressure reconstructions for the European–North Atlantic region for the period
724 1850–2003. *Journal of Climate*, **19**, 2717–2742. URL: <https://doi.org/10.1175/JCLI3775.1>.
- 725 Bengtsson, L., Hagemann, S. and Hodges, K. I. (2004) Can climate trends be calculated from reanalysis data? *Journal of Geo-*
726 *physical Research: Atmospheres*, **109**. URL: <https://agupubs.onlinelibrary.wiley.com/doi/abs/10.1029/2004JD004536>.
- 727 van den Besselaar, E. J. M., Haylock, M. R., van der Schrier, G. and Klein Tank, A. M. G. (2011) A European daily high-resolution
728 observational gridded data set of sea level pressure. *Journal of Geophysical Research: Atmospheres*, **116**.

- 729 Bloom, S. C., Takacs, L. L., da Silva, A. M. and Ledvina, D. (1996) Data assimilation using incremental analysis updates. *Monthly*
730 *Weather Review*, **124**, 1256–1271. URL: [https://doi.org/10.1175/1520-0493\(1996\)124<1256:DAUIAU>2.0.CO;2](https://doi.org/10.1175/1520-0493(1996)124<1256:DAUIAU>2.0.CO;2).
- 731 Bosilovich, M. G., Robertson, F. R. and Chen, J. (2011) Global energy and water budgets in MERRA. *Journal of Climate*, **24**,
732 5721–5739. URL: <https://doi.org/10.1175/2011JCLI4175.1>.
- 733 Brohan, P., Compo, G. P., Brönnimann, S., Allan, R. J., Auchmann, R., Brugnara, Y., Sardeshmukh, P. D. and Whitaker, J. S. (2016)
734 The 1816 ‘year without a summer’ in an atmospheric reanalysis. *Climate Past Discuss*, **2016**, 1–11.
- 735 Brönnimann, S., Brugnara, Y., Allan, R. J., Brunet, M., Compo, G. P., Crouthamel, R. I., Jones, P. D., Jourdain, S., Luterbacher, J.,
736 Siegmund, P., Valente, M. A. and Wilkinson, C. W. (2018) A roadmap to climate data rescue services. *Geoscience Data Journal*,
737 **5**, 28–39. URL: <https://rmets.onlinelibrary.wiley.com/doi/abs/10.1002/gdj3.56>.
- 738 Brönnimann, S., Grant, A. N., Compo, G. P., Ewen, T., Griesser, T., Fischer, A. M., Schraner, M. and Stickler, A. (2012) A multi-data
739 set comparison of the vertical structure of temperature variability and change over the Arctic during the past 100 years.
740 *Climate Dynamics*, **39**, 1577–1598. URL: <https://doi.org/10.1007/s00382-012-1291-6>.
- 741 Burn, M. J. and Palmer, S. E. (2015) Atlantic hurricane activity during the last millennium. *Scientific reports*, **5**, 12838.
- 742 Compo, G. P., Sardeshmukh, P. D. and Penland, C. (2001) Changes of subseasonal variability associated with El Niño. *Journal of*
743 *climate*, **14**, 3356–3374.
- 744 Compo, G. P., Sardeshmukh, P. D., Whitaker, J. S., Brohan, P., Jones, P. D. and McColl, C. (2013) Independent confirmation of
745 global land warming without the use of station temperatures. *Geophysical Research Letters*, **40**, 3170–3174. URL: <https://agupubs.onlinelibrary.wiley.com/doi/abs/10.1002/grl.50425>.
- 746 //agupubs.onlinelibrary.wiley.com/doi/abs/10.1002/grl.50425.
- 747 Compo, G. P., Whitaker, J. S. and Sardeshmukh, P. D. (2006) Feasibility of a 100-year reanalysis using only surface pressure
748 data. *Bulletin of the American Meteorological Society*, **87**, 175–190.
- 749 Compo, G. P., Whitaker, J. S., Sardeshmukh, P. D., Allan, R. J., McColl, C., Yin, X., Vose, R. S., Matsui, N., Ashcroft, L., Auchmann,
750 R., Benoy, M., Bessemoulin, P., Brandsma, T., Brohan, P., Brunet, M., Comeaux, J., Cram, T. A., Crouthamel, R., Groisman, P. Y.,
751 Hersbach, H., Jones, P. D., Jonsson, T., Jourdain, S., Kelly, G., Knapp, K. R., Kruger, A., Kubota, H., Lentini, G., Lorrey, A., Lott,
752 N., Lubker, S. J., Luterbacher, J., Marshall, G. J., Maugeri, M., Mock, C. J., Mok, H. Y., Nordli, O., Przybylak, R., Rodwell, M. J.,
753 Ross, T. F., Schuster, D., Srncic, L., Valente, M. A., Vizi, Z., Wang, X. L., Westcott, N., Woollen, J. S. and Worley, S. J. (2015) The
754 international surface pressure databank version 3. URL: <https://doi.org/10.5065/D6D50K29>.
- 755 Compo, G. P., Whitaker, J. S., Sardeshmukh, P. D., Matsui, N., Allan, R. J., Yin, X., Gleason, B. E., Vose, R. S., Rutledge, G., Besse-
756 moulin, P. et al. (2011) The twentieth century reanalysis project. *Quarterly Journal of the Royal Meteorological Society*, **137**,
757 1–28.
- 758 Cram, T. A., Compo, G. P., Yin, X., Allan, R. J., McColl, C., Vose, R. S., Whitaker, J. S., Matsui, N., Ashcroft, L., Auchmann, R.,
759 Bessemoulin, P., Brandsma, T., Brohan, P., Brunet, M., Comeaux, J., Crouthamel, R., Gleason, B. E., Groisman, P. Y., Hersbach,
760 H., Jones, P. D., Jónsson, T., Jourdain, S., Kelly, G., Knapp, K. R., Kruger, A., Kubota, H., Lentini, G., Lorrey, A., Lott, N., Lubker,
761 S. J., Luterbacher, J., Marshall, G. J., Maugeri, M., Mock, C. J., Mok, H. Y., Nordli, Ø., Rodwell, M. J., Ross, T. F., Schuster, D.,
762 Srncic, L., Valente, M. A., Vizi, Z., Wang, X. L., Westcott, N., Woollen, J. S. and Worley, S. J. (2015) The International Surface
763 Pressure Databank version 2. *Geoscience Data Journal*, **2**, 31–46.
- 764 Daley, R. (1993) *Atmospheric data analysis*. No. 2. Cambridge University Press.
- 765 Dee, D. P., Uppala, S., Simmons, A., Berrisford, P., Poli, P., Kobayashi, S., Andrae, U., Balmaseda, M., Balsamo, G., Bauer, d. P. et al.
766 (2011) The ERA-Interim reanalysis: Configuration and performance of the data assimilation system. *Quarterly Journal of the*
767 *royal meteorological society*, **137**, 553–597.
- 768 Deser, C., Simpson, I. R., McKinnon, K. A. and Phillips, A. S. (2017) The Northern Hemisphere extratropical atmospheric circula-
769 tion response to ENSO: How well do we know it and how do we evaluate models accordingly? *Journal of Climate*, **30**,
770 5059–5082.

- 771 Desroziers, G., Berre, L., Chapnik, B. and Poli, P. (2005) Diagnosis of observation, background and analysis error statistics in
772 observation space. *Quarterly Journal of the Royal Meteorological Society*, **131**, 3385–3396. URL: <http://doi.org/10.1256/qj.05.108>.
- 773
- 774 Diamond, H., Lorrey, A., Knapp, K. and Levinson, D. (2012) Development of an enhanced tropical cyclone tracks database for
775 the southwest Pacific from 1840 to 2010. *International Journal of Climatology*, **32**, 2240–2250.
- 776 Diaz, H., Folland, C., Manabe, T., Parker, D., Reynolds, R. and Woodruff, S. (2002) Workshop on advances in the use of historical
777 marine climate data. *Bulletin of the World Meteorological Organization*, **51**, 377–379.
- 778 Donat, M. G., Alexander, L. V., Herold, N. and Dittus, A. J. (2016) Temperature and precipitation extremes in century-long
779 gridded observations, reanalyses, and atmospheric model simulations. *Journal of Geophysical Research: Atmospheres*, **121**,
780 11,174–11,189. URL: <https://agupubs.onlinelibrary.wiley.com/doi/abs/10.1002/2016JD025480>.
- 781 Ferguson, C. R. and Villarini, G. (2012) Detecting inhomogeneities in the Twentieth Century Reanalysis over the central United
782 States. *Journal of Geophysical Research: Atmospheres*, **117**. URL: <https://agupubs.onlinelibrary.wiley.com/doi/abs/10.1029/2011JD016988>.
- 783
- 784 Freeman, E., Woodruff, S. D., Worley, S. J., Lubker, S. J., Kent, E. C., Angel, W. E., Berry, D. I., Brohan, P., Eastman, R., Gates, L. et al.
785 (2017) ICOADS Release 3.0: a major update to the historical marine climate record. *International Journal of Climatology*, **37**,
786 2211–2232.
- 787 Fujiwara, M., Wright, J. S., Manney, G. L., Gray, L. J., Anstey, J., Birner, T., Davis, S., Gerber, E. P., Harvey, V. L., Hegglin, M. I.,
788 Homeyer, C. R., Knox, J. A., Krüger, K., Lambert, A., Long, C. S., Martineau, P., Molod, A., Monge-Sanz, B. M., Santee, M. L.,
789 Tegtmeier, S., Chabrillat, S., Tan, D. G. H., Jackson, D. R., Polavarapu, S., Compo, G. P., Dragani, R., Ebisuzaki, W., Harada,
790 Y., Kobayashi, C., McCarty, W., Onogi, K., Pawson, S., Simmons, A., Wargan, K., Whitaker, J. S. and Zou, C.-Z. (2017) Intro-
791 duction to the SPARC Reanalysis Intercomparison Project (S-RIP) and overview of the reanalysis systems. *Atmospheric*
792 *Chemistry and Physics*, **17**, 1417–1452. URL: <https://www.atmos-chem-phys.net/17/1417/2017/>.
- 793 Gaspari, G. and Cohn, S. E. (1999) Construction of correlation functions in two and three dimensions. *Quarterly Journal of the*
794 *Royal Meteorological Society*, **125**, 723–757.
- 795 Gelaro, R., McCarty, W., Suárez, M. J., Todling, R., Molod, A., Takacs, L., Randles, C. A., Darmenov, A., Bosilovich, M. G., Reichle,
796 R., Wargan, K., Coy, L., Cullather, R., Draper, C., Akella, S., Buchard, V., Conaty, A., da Silva, A. M., Gu, W., Kim, G.-K., Koster, R.,
797 Lucchesi, R., Merkova, D., Nielsen, J. E., Partyka, G., Pawson, S., Putman, W., Rienecker, M., Schubert, S. D., Sienkiewicz, M.
798 and Zhao, B. (2017) The Modern-Era Retrospective Analysis for Research and Applications, Version 2 (MERRA-2). *Journal*
799 *of Climate*, **30**, 5419–5454.
- 800 Giese, B. S., Compo, G. P., Slowey, N. C., Sardeshmukh, P. D., Carton, J. A., Ray, S. and Whitaker, J. S. (2010) The 1918/19 El Niño.
801 *Bulletin of the American Meteorological Society*, **91**, 177–183,148. URL: [https://search.proquest.com/docview/232619945?](https://search.proquest.com/docview/232619945?accountid=28266)
802 [accountid=28266](https://search.proquest.com/docview/232619945?accountid=28266).
- 803 Giese, B. S., Seidel, H. F., Compo, G. P. and Sardeshmukh, P. D. (2016) An ensemble of ocean reanalyses for 1815–2013
804 with sparse observational input. *Journal of Geophysical Research: Oceans*, **121**, 6891–6910. URL: [https://agupubs.](https://agupubs.onlinelibrary.wiley.com/doi/abs/10.1002/2016JC012079)
805 [onlinelibrary.wiley.com/doi/abs/10.1002/2016JC012079](https://agupubs.onlinelibrary.wiley.com/doi/abs/10.1002/2016JC012079).
- 806 Häkkinen, S., Rhines, P. B. and Worthen, D. L. (2011) Atmospheric blocking and Atlantic multidecadal ocean variability. *Science*,
807 **334**, 655–659. URL: <http://science.sciencemag.org/content/334/6056/655>.
- 808 Hamill, T. M., Whitaker, J. S. and Snyder, C. (2001) Distance-dependent filtering of background error covariance estimates in
809 an ensemble Kalman filter. *Monthly Weather Review*, **129**, 2776–2790.
- 810 Harris, L. M. and Lin, S.-J. (2013) A two-way nested global-regional dynamical core on the cubed-sphere grid. *Monthly Weather*
811 *Review*, **141**, 283–306.
- 812 Harvey, T., Renwick, J. A., Lorrey, A. M. and Ngari, A. (2019) The representation of the South Pacific Convergence Zone in the
813 20th Century Reanalysis. *Monthly Weather Review*, **0**, null. In press.

- 814 Hegerl, G. C., Brönnimann, S., Schurer, A. and Cowan, T. (2018) The early 20th century warming: Anomalies, causes, and con-
815 sequences. *Wiley Interdisciplinary Reviews: Climate Change*, **9**, e522. URL: [https://onlinelibrary.wiley.com/doi/abs/10.](https://onlinelibrary.wiley.com/doi/abs/10.1002/wcc.522)
816 [1002/wcc.522](https://onlinelibrary.wiley.com/doi/abs/10.1002/wcc.522).
- 817 Houtekamer, P. L. and Mitchell, H. L. (1998) Data assimilation using an ensemble Kalman filter technique. *Monthly Weather*
818 *Review*, **126**, 796–811.
- 819 – (2001) A sequential ensemble Kalman filter for atmospheric data assimilation. *Monthly Weather Review*, **129**, 123–137.
- 820 Huang, J., Ji, M., Xie, Y., Wang, S., He, Y. and Ran, J. (2016) Global semi-arid climate change over last 60 years. *Climate Dynamics*,
821 **46**, 1131–1150. URL: <https://doi.org/10.1007/s00382-015-2636-8>.
- 822 Huang, J., Xie, Y., Guan, X., Li, D. and Ji, F. (2017) The dynamics of the warming hiatus over the Northern Hemisphere. *Climate*
823 *Dynamics*, **48**, 429–446. URL: <https://doi.org/10.1007/s00382-016-3085-8>.
- 824 Huang, X.-Y. and Lynch, P. (1993) Diabatic digital-filtering initialization: Application to the HIRLAM model. *Monthly Weather*
825 *Review*, **121**, 589–603. URL: [https://doi.org/10.1175/1520-0493\(1993\)121<0589:DDFIAT>2.0.CO;2](https://doi.org/10.1175/1520-0493(1993)121<0589:DDFIAT>2.0.CO;2).
- 826 Janjić, T. and Cohn, S. E. (2006) Treatment of observation error due to unresolved scales in atmospheric data assimilation.
827 *Monthly Weather Review*, **134**, 2900–2915.
- 828 Jones, P., Harpham, C. and Briffa, K. (2013) Lamb weather types derived from reanalysis products. *International Journal of*
829 *Climatology*, **33**, 1129–1139.
- 830 Jones, P. D., Harpham, C. and Lister, D. (2016) Long-term trends in gale days and storminess for the falkland islands. *Interna-*
831 *tional Journal of Climatology*, **36**, 1413–1427.
- 832 Kalnay, E., Kanamitsu, M., Kistler, R., Collins, W., Deaven, D., Gandin, L., Iredell, M., Saha, S., White, G., Woollen, J. et al. (1996)
833 The NCEP/NCAR 40-year reanalysis project. *Bulletin of the American Meteorological Society*, **77**, 437–472.
- 834 Kent, E. C., Fangohr, S. and Berry, D. I. (2013) A comparative assessment of monthly mean wind speed products over the global
835 ocean. *International Journal of Climatology*, **33**, 2520–2541. URL: [https://rmets.onlinelibrary.wiley.com/doi/abs/10.](https://rmets.onlinelibrary.wiley.com/doi/abs/10.1002/joc.3606)
836 [1002/joc.3606](https://rmets.onlinelibrary.wiley.com/doi/abs/10.1002/joc.3606).
- 837 Kinter III, J., Fennessy, M., Krishnamurthy, V. and Marx, L. (2004) An evaluation of the apparent interdecadal shift in the tropical
838 divergent circulation in the NCEP–NCAR reanalysis. *Journal of Climate*, **17**, 349–361.
- 839 Kistler, R., Kalnay, E., Collins, W., Saha, S., White, G., Woollen, J., Chelliah, M., Ebisuzaki, W., Kanamitsu, M., Kousky, V. et al.
840 (2001) The NCEP–NCAR 50-year reanalysis: monthly means CD-ROM and documentation. *Bulletin of the American Mete-*
841 *orological society*, **82**, 247–268.
- 842 Klotzbach, P. J., Oliver, E. C. J., Leeper, R. D. and Schreck, C. J. (2016) The relationship between the Madden-Julian Oscillation
843 (MJO) and southeastern New England snowfall. *Monthly Weather Review*, **144**, 1355–1362. URL: [https://doi.org/10.](https://doi.org/10.1175/MWR-D-15-0434.1)
844 [1175/MWR-D-15-0434.1](https://doi.org/10.1175/MWR-D-15-0434.1).
- 845 Knapp, K. R., Kruk, M. C., Levinson, D. H., Diamond, H. J. and Neumann, C. J. (2010) The international best track archive for
846 climate stewardship (IBTrACS) unifying tropical cyclone data. *Bulletin of the American Meteorological Society*, **91**, 363–376.
- 847 Kobayashi, S., Ota, Y., Harada, Y., Ebata, A., Moriya, M., Onoda, H., Onogi, K., Kamahori, H., Kobayashi, C., Endo, H. et al. (2015)
848 The JRA-55 reanalysis: General specifications and basic characteristics. *Journal of the Meteorological Society of Japan. Ser. II*,
849 **93**, 5–48.
- 850 Kruk, M. C., Knapp, K. R. and Levinson, D. H. (2010) A technique for combining global tropical cyclone best track data. *Journal*
851 *of Atmospheric and Oceanic Technology*, **27**, 680–692.
- 852 Kubota, H. (2012) Variability of typhoon tracks and genesis over the Western North Pacific. *Cyclones: Formation, Triggers and*
853 *Control*, Nova Science Publishers, Inc, 95–114.

- 854 Kwon, J., Yi, J.-W. and Song, S. M. (2004) Adaptive cubic interpolation of CT slices for maximum intensity projections. In *Medical*
855 *Imaging 2004: Visualization, Image-Guided Procedures, and Display*, vol. 5367, 837–845. International Society for Optics and
856 Photonics.
- 857 Laloyaux, P., de Boisseson, E., Balmaseda, M., Bidlot, J.-R., Broennimann, S., Buizza, R., Dalhgren, P., Dee, D., Haimberger, L.,
858 Hersbach, H. et al. (2018) CERA-20C: A coupled reanalysis of the Twentieth Century. *Journal of Advances in Modeling Earth*
859 *Systems*, **10**, 1172–1195.
- 860 Landschützer, P., Gruber, N., Haumann, F. A., Rödenbeck, C., Bakker, D. C. E., van Heuven, S., Hoppema, M., Metzl, N., Sweeney,
861 C., Takahashi, T., Tilbrook, B. and Wanninkhof, R. (2015) The reinvigoration of the Southern Ocean carbon sink. *Science*,
862 **349**, 1221–1224. URL: <http://science.sciencemag.org/content/349/6253/1221>.
- 863 Lei, L. and Whitaker, J. S. (2016) A four-dimensional incremental analysis update for the ensemble Kalman filter. *Monthly*
864 *Weather Review*, **144**, 2605–2621.
- 865 van Loon, H. and Jenne, R. L. (1972) The zonal harmonic standing waves in the southern hemisphere. *Journal of Geophysical*
866 *Research*, **77**, 992–1003. URL: <https://agupubs.onlinelibrary.wiley.com/doi/abs/10.1029/JC077i006p00992>.
- 867 Lorenc, A. C. (1986) Analysis methods for numerical weather prediction. *Quarterly Journal of the Royal Meteorological Society*,
868 **112**, 1177–1194. URL: <https://rmets.onlinelibrary.wiley.com/doi/abs/10.1002/qj.49711247414>.
- 869 Lorrey, A., Dalu, G., Renwick, J., Diamond, H. and Gaetani, M. (2012) Reconstructing the South Pacific Convergence Zone posi-
870 tion during the Presatellite Era: A La Niña case study. *Monthly Weather Review*, **140**, 3653–3668.
- 871 Lorrey, A. M. and Chappell, P. R. (2016) The “dirty weather” diaries of Reverend Richard Davis: insights about early colonial-era
872 meteorology and climate variability for northern New Zealand, 1839–1851. *Climate of the Past*, **12**, 553–553.
- 873 Lott, N., Vose, R., Del Greco, S., Ross, T., Worley, S. and Comeaux, J. (2008) The integrated surface database: partnerships and
874 progress. In *Extended Abstracts, 24th Conf. on Interactive Information and Processing Systems*.
- 875 Lynch, P. and Huang, X.-Y. (1992) Initialization of the HIRLAM model using a digital filter. *Monthly Weather Review*, **120**, 1019–
876 1034. URL: [https://doi.org/10.1175/1520-0493\(1992\)120<1019: IOTHMU>2.0.CO;2](https://doi.org/10.1175/1520-0493(1992)120<1019: IOTHMU>2.0.CO;2).
- 877 Middleton, K. (1964) *The history of the barometer*. Johns Hopkins University Press.
- 878 Monmonier, M. (1999) *Air apparent: How meteorologists learned to map, predict, and dramatize weather*. University of Chicago
879 Press.
- 880 Moore, G. and Babij, M. (2017) Iceland’s Great Frost Winter of 1917/1918 and its representation in reanalyses of the twentieth
881 century. *Quarterly Journal of the Royal Meteorological Society*, **143**, 508–520.
- 882 Morice, C. P., Kennedy, J. J., Rayner, N. A. and Jones, P. D. (2012) Quantifying uncertainties in global and regional temperature
883 change using an ensemble of observational estimates: The hadcrut4 data set. *Journal of Geophysical Research: Atmospheres*,
884 **117**. URL: <https://agupubs.onlinelibrary.wiley.com/doi/abs/10.1029/2011JD017187>.
- 885 Mueller, W. A., Pohlmann, H., Sienz, F. and Smith, D. (2014) Decadal climate predictions for the period 1901–2010 with a
886 coupled climate model. *Geophysical Research Letters*, **41**, 2100–2107.
- 887 Paik, S. and Min, S.-K. (2017) Climate responses to volcanic eruptions assessed from observations and CMIP5 multi-models.
888 *Climate Dynamics*, **48**, 1017–1030. URL: <https://doi.org/10.1007/s00382-016-3125-4>.
- 889 Parker, W. S. (2016) Reanalyses and observations: What’s the difference? *Bulletin of the American Meteorological Society*, **97**,
890 1565–1572.
- 891 Poli, P., Hersbach, H., Berrisford, P. and other authors (2015) ERA-20C Deterministic. Shinfield Park, Reading.

- 892 Poli, P., Hersbach, H., Dee, D. P., Berrisford, P., Simmons, A. J., Vitart, F., Laloyaux, P., Tan, D. G., Peubey, C., Thépaut, J.-N. et al.
893 (2016) ERA-20C: An atmospheric reanalysis of the twentieth century. *Journal of Climate*, **29**, 4083–4097.
- 894 Raphael, M. N. (2004) A zonal wave 3 index for the Southern Hemisphere. *Geophysical Research Letters*, **31**. URL: [https://](https://agupubs.onlinelibrary.wiley.com/doi/abs/10.1029/2004GL020365)
895 agupubs.onlinelibrary.wiley.com/doi/abs/10.1029/2004GL020365.
- 896 Rayner, N. A., Brohan, P., Parker, D. E., Folland, C. K., Kennedy, J. J., Vanicek, M., Ansell, T. J. and Tett, S. F. B. (2006) Improved
897 analyses of changes and uncertainties in sea surface temperature measured in situ since the mid-nineteenth century: The
898 HadSST2 dataset. *Journal of Climate*, **19**, 446–469. URL: <https://doi.org/10.1175/JCLI3637.1>.
- 899 Rohrer, M., Brönnimann, S., Martius, O., Raible, C. C., Wild, M. and Compo, G. P. (2018) Representation of extratropical cy-
900 clones, blocking anticyclones, and alpine circulation types in multiple reanalyses and model simulations. *Journal of Climate*,
901 **31**, 3009–3031. URL: <https://doi.org/10.1175/JCLI-D-17-0350.1>.
- 902 Slivinski, L. C. (2018) Historical reanalysis: What, how, and why? *Journal of Advances in Modeling Earth Systems*, **10**, 1736–1739.
903 URL: <https://agupubs.onlinelibrary.wiley.com/doi/abs/10.1029/2018MS001434>.
- 904 Slonosky, V. C. and Graham, E. (2005) Canadian pressure observations and circulation variability: Links to air temperature.
905 *International Journal of Climatology: A Journal of the Royal Meteorological Society*, **25**, 1473–1492.
- 906 Smith, A., Lott, N. and Vose, R. (2011) The integrated surface database: Recent developments and partnerships. *Bulletin of the*
907 *American Meteorological Society*, **92**, 704–708.
- 908 Spencer, L., McColl, C., Brohan, P., Wood, K., Allan, R. and Compo, G. P. (2019) OldWeather3 marine data for ICOADS input.
909 <https://doi.org/10.5065/Q54H-3R61>.
- 910 Titchner, H. A. and Rayner, N. A. (2014) The Met Office Hadley Centre sea ice and sea surface temperature data set, ver-
911 sion 2: 1. Sea ice concentrations. *Journal of Geophysical Research: Atmospheres*, **119**, 2864–2889. URL: [https://agupubs.](https://agupubs.onlinelibrary.wiley.com/doi/abs/10.1002/2013JD020316)
912 [onlinelibrary.wiley.com/doi/abs/10.1002/2013JD020316](https://agupubs.onlinelibrary.wiley.com/doi/abs/10.1002/2013JD020316).
- 913 Trenberth, K. E. and Paolino, D. A. (1980) The Northern Hemisphere sea-level pressure data set: Trends, errors and disconti-
914 nuities. *Monthly Weather Review*, **108**, 855–872. URL: [https://doi.org/10.1175/1520-0493\(1980\)108<0855:TNHSLP>2.0.](https://doi.org/10.1175/1520-0493(1980)108<0855:TNHSLP>2.0.CO;2)
915 [CO;2](https://doi.org/10.1175/1520-0493(1980)108<0855:TNHSLP>2.0.CO;2).
- 916 Trenberth, K. E. and Smith, L. (2005) The mass of the atmosphere: A constraint on global analyses. *Journal of Climate*, **18**,
917 864–875.
- 918 Walsh, J. E., Chapman, W. L. and Fetterer, F. (2015, updated 2016) Gridded monthly sea ice extent and concentration, 1850
919 onward, version 1. Boulder, Colorado USA. NSIDC: National Snow and Ice Data Center.
- 920 Wang, X. L., Feng, Y., Chan, R. and Isaac, V. (2016) Inter-comparison of extra-tropical cyclone activity in nine reanalysis datasets.
921 *Atmospheric Research*, **181**, 133 – 153.
- 922 Wang, X. L., Feng, Y., Compo, G. P., Swail, V. R., Zwiers, F. W., Allan, R. J. and Sardeshmukh, P. D. (2013) Trends and low frequency
923 variability of extra-tropical cyclone activity in the ensemble of twentieth century reanalysis. *Climate Dynamics*, **40**, 2775–
924 2800.
- 925 Whitaker, J. S., Compo, G. P., Wei, X. and Hamill, T. M. (2004) Reanalysis without radiosondes using ensemble data assimilation.
926 *Monthly Weather Review*, **132**, 1190–1200.
- 927 Whitaker, J. S. and Hamill, T. M. (2002) Ensemble data assimilation without perturbed observations. *Monthly Weather Review*,
928 **130**, 1913–1924.
- 929 – (2012) Evaluating methods to account for system errors in ensemble data assimilation. *Monthly Weather Review*, **140**, 3078–
930 3089.

- 931 Woodruff, S. D., Worley, S. J., Lubker, S. J., Ji, Z., Eric Freeman, J., Berry, D. I., Brohan, P., Kent, E. C., Reynolds, R. W., Smith, S. R.
932 et al. (2011) ICOADS Release 2.5: extensions and enhancements to the surface marine meteorological archive. *International journal of climatology*, **31**, 951–967.
933
- 934 Worley, S. J., Woodruff, S. D., Reynolds, R. W., Lubker, S. J. and Lott, N. (2005) ICOADS release 2.1 data and products. *International Journal of Climatology*, **25**, 823–842. URL: <https://rmets.onlinelibrary.wiley.com/doi/abs/10.1002/joc.1166>.
935
- 936 Zhang, L., Kumar, A. and Wang, W. (2012) Influence of changes in observations on precipitation: A case study for the Cli-
937 mate Forecast System Reanalysis (CFSR). *Journal of Geophysical Research: Atmospheres*, **117**. URL: [https://agupubs.
938 onlinelibrary.wiley.com/doi/abs/10.1029/2011JD017347](https://agupubs.onlinelibrary.wiley.com/doi/abs/10.1029/2011JD017347).

Author Manuscript

TABLE 1 Platform-dependent baseline observation errors used in the 20CRv3 system (in hPa). Note that only surface pressure data are assimilated, including from radiosonde and dropsonde observing platforms. 'SLP only' refers to stations that do not report surface pressure, only sea level pressure.

Type	Error (hPa)
radiosonde	1.2
dropsonde	2.0
marine	2.0
station	1.2
station (SLP only)	1.6
tropical cyclones	2.5

SLP, sea level pressure.

TABLE 2 Covariance inflation parameters used in 20CRv2c as a function of latitude and year. A value of 1 corresponds to no inflation. NH=90°N–30°N; Tropics = 30°N–30°S; SH = 30°S–90°S.

years	NH	Tropics	SH
1851 – 1870	1.01	1.01	1.01
1871 – 1890	1.05	1.01	1.01
1891 – 1920	1.09	1.02	1.01
1921 – 1950	1.12	1.03	1.02
1951 – 2014	1.12	1.07	1.07

NH, Northern Hemisphere; SH, Southern Hemisphere.

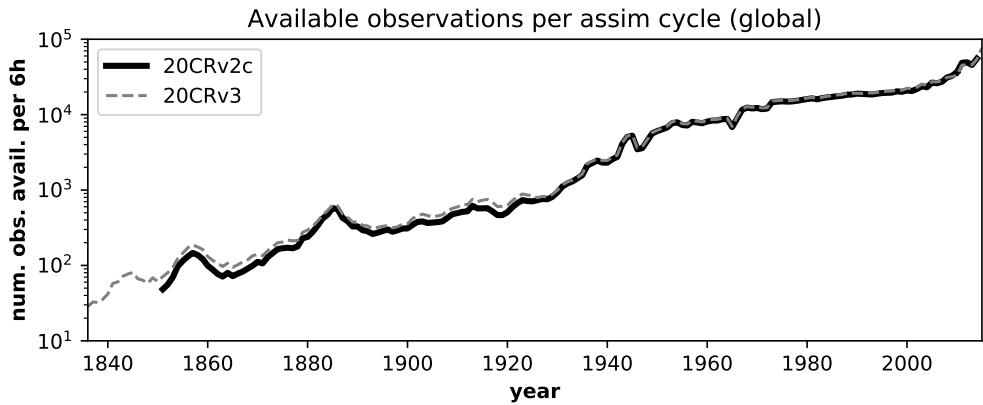


FIGURE 1 Time series of the annual average number of observations available to be assimilated globally per 6-hour window within 20CRv2c (ISPDv3.2.9, solid black) and 20CRv3 (ISPDv4.7, dashed gray).

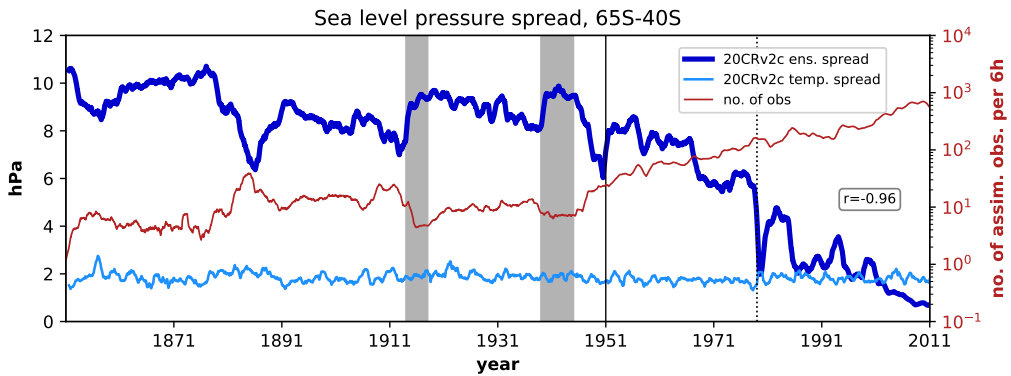


FIGURE 2 Time series of ensemble spread (thick dark blue curve) and temporal spread of the ensemble mean (thin light blue curve) for sea level pressure from 20CRv2c averaged over the zonal band from 65°S to 40°S. Number of observations assimilated per 6-hour window in this region is shown in red (right hand axis). A 1-year running average was applied to all curves. Correlation r is calculated between the smoothed ensemble spread and the smoothed logarithm of the number of assimilated observations. Notable years are emphasized with vertical lines and shading; see text for details.

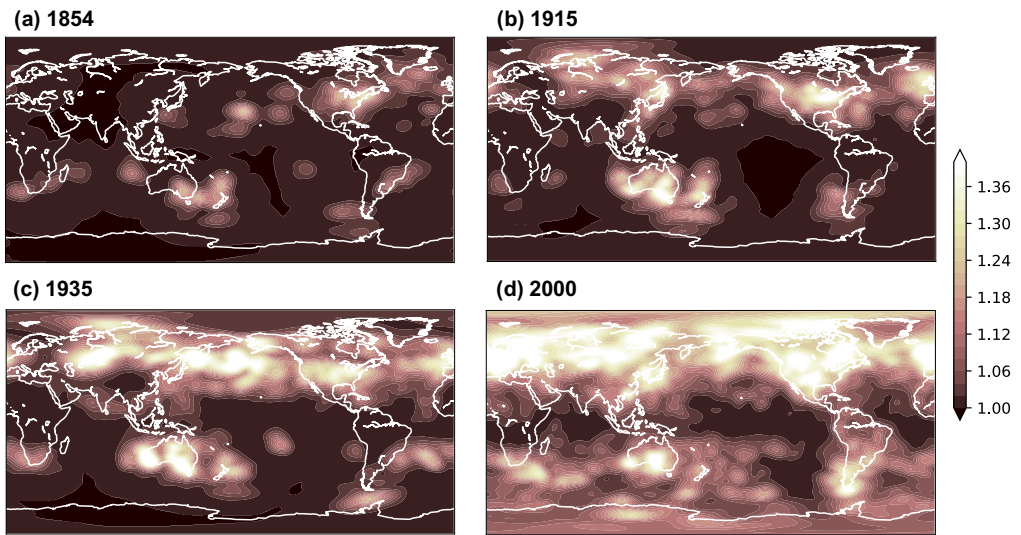


FIGURE 3 Maps of the adaptive inflation parameter λ_{inf} (unitless) used in the 20CRv3 system for 0000 UTC on 1 Sept in (a) 1854; (b) 1915; (c) 1935; and (d) 2000. A value of 1 corresponds to no inflation. Note the relationship of λ_{inf} with the observation network density.

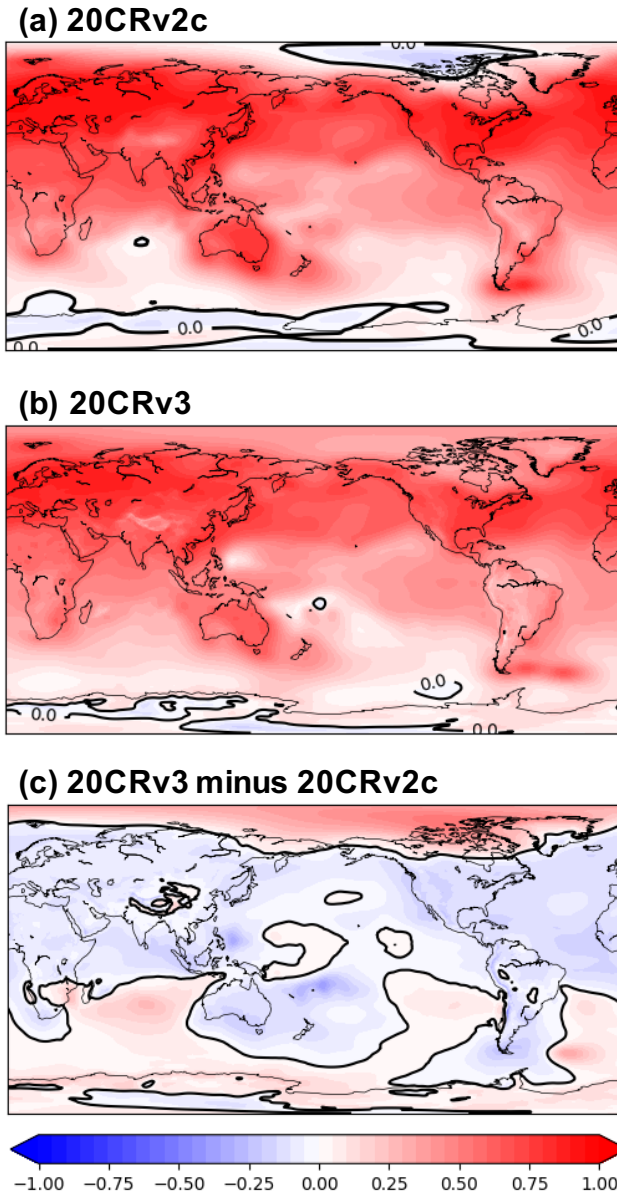


FIGURE 4 Maps of normalized confidence of SLP averaged over JFM for 1916-1918 from (a) 20CRv2c and (b) 20CRv3, as well as (c) the difference (20CRv3 minus 20CRv2c). In (a)-(b), zero (black contour) represents climatological uncertainty, blue represents less certainty than climatology, and red represents more certainty. In (c), red represents an increase in confidence from 20CRv2c to 20CRv3, and blue a decrease.

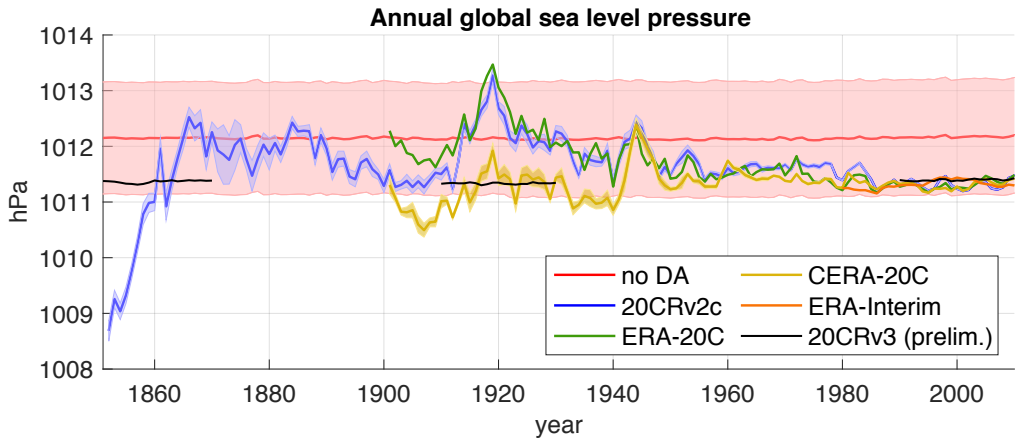


FIGURE 5 Time series of annually-averaged global SLP from several reanalyses, as well as a non-assimilating ensemble of model runs.

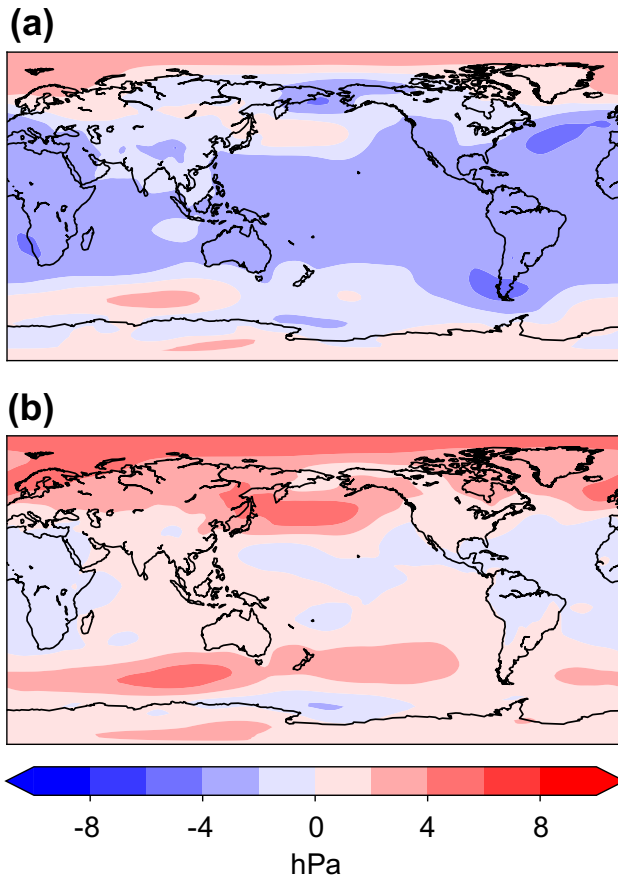


FIGURE 6 Maps of analyzed sea level pressure anomalies (with respect to the analyzed 20CRv2c 1981–2010 climatology) for 1851–1853 of (a) 20CRv2c and (b) an identical experiment with the 20CRv2c system that assimilated 10% fewer ship observations.

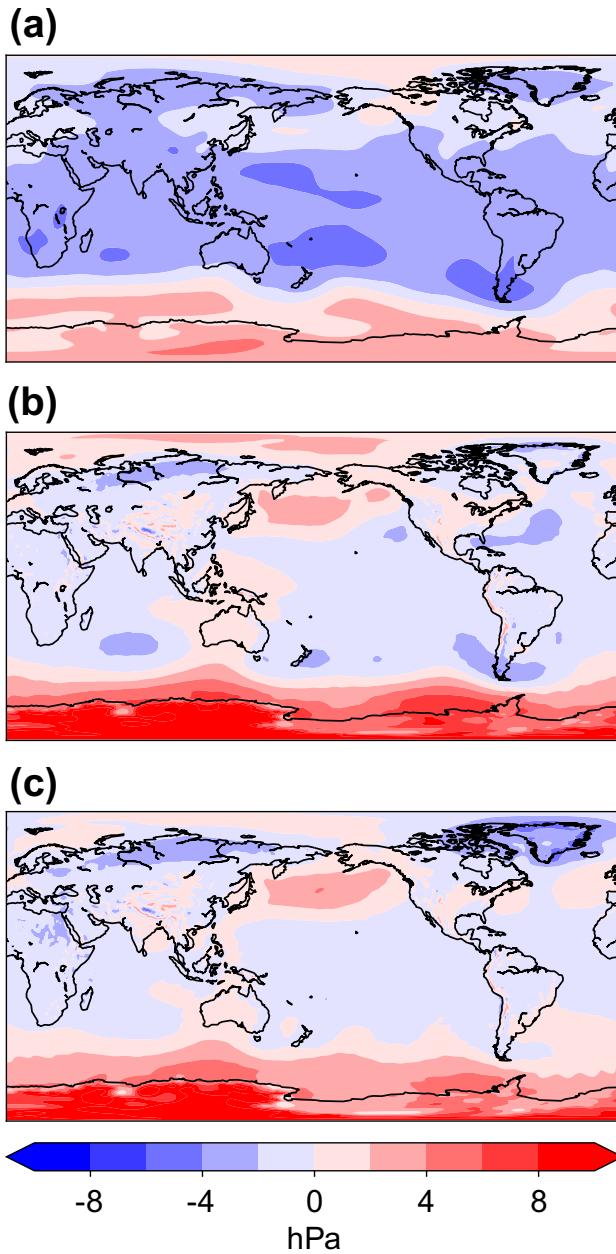


FIGURE 7 Maps of the year 1854 annually-averaged sea level pressure anomaly (with respect to the 1981-2010 climatology) of (a) 20CRv2c (without dry air mass specification), (b) preliminary version 3 tests without ship bias correction (with dry air mass specification), and (c) preliminary version 3 tests with ship bias correction (with dry air mass specification).

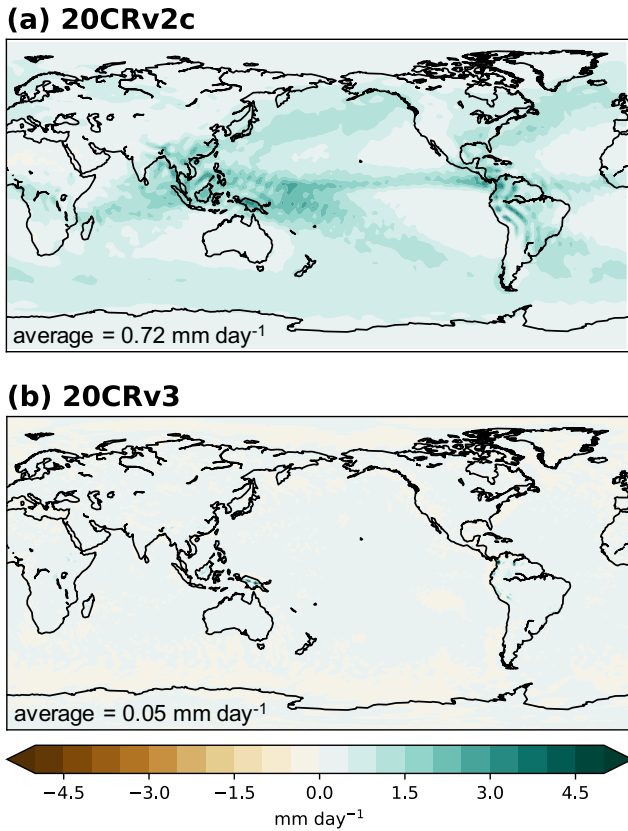


FIGURE 8 Maps of the year 2002 annually-averaged differences (mm day⁻¹) between 3-6 hour forecasted precipitation rate and 0-3 hour forecasted precipitation rate in (a) 20CRv2c (which uses the digital filter) and (b) 20CRv3 (which uses the IAU instead of the digital filter). In a perfect system, these differences would be approximately zero.

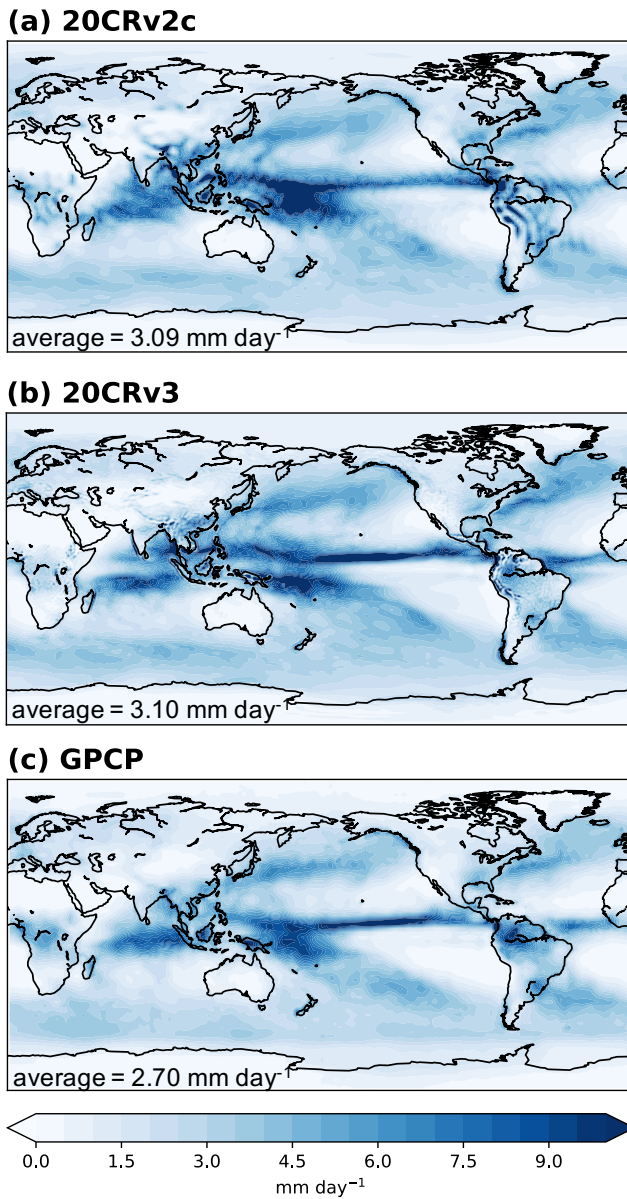


FIGURE 9 Maps of the year 2002 annually-averaged forecasted precipitation rate (mm day⁻¹) in (a) 20CRv2c, (b) 20CRv3, and (c) the GPCP satellite/gauge blended fields.

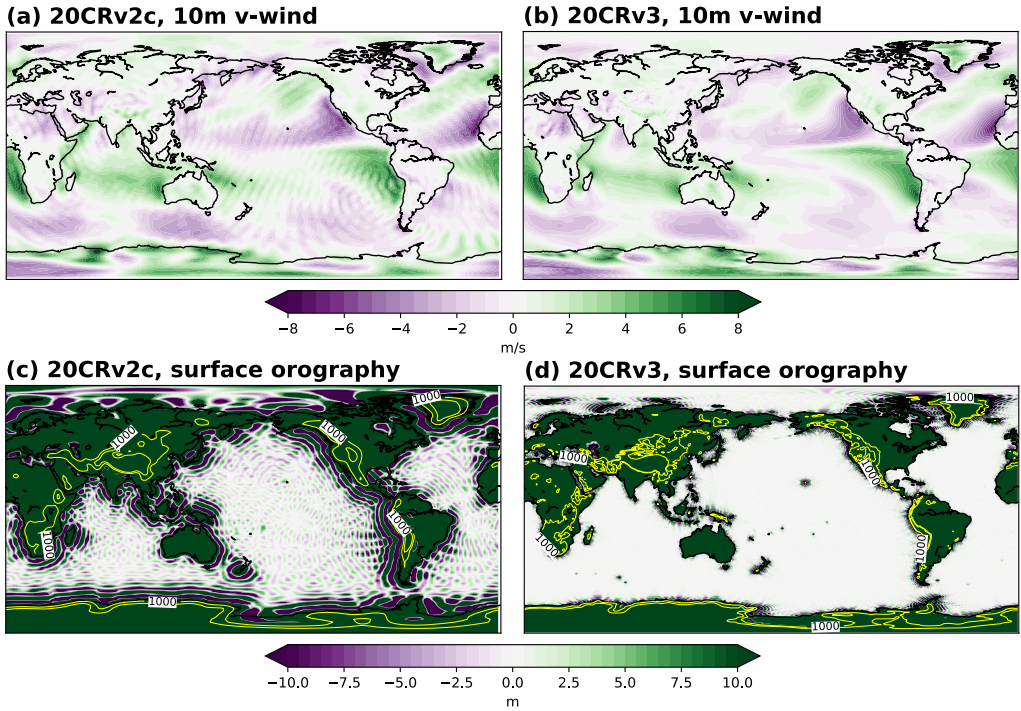


FIGURE 10 Maps of the year 2002 annual average of 10-meter meridional wind fields (top row, ms^{-1}) and surface orography fields (bottom row, m) from 20CRv2c (left) and 20CRv3 (right). The 1000 m and 2000 m contours have been plotted in yellow in (c) and (d), with the 1000 m contour labeled.

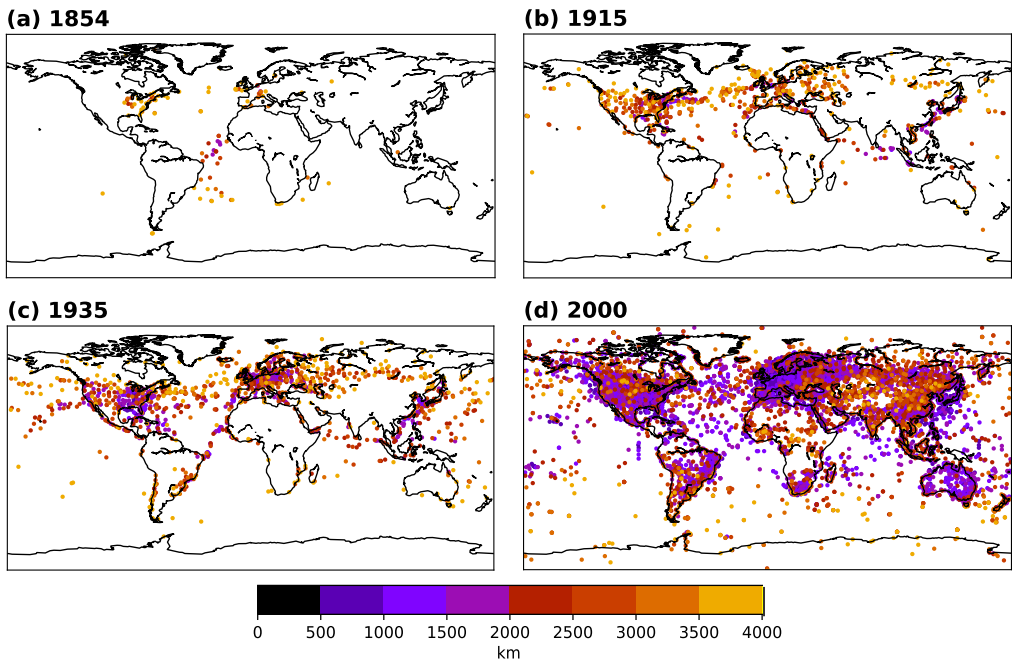


FIGURE 11 Localization values (km) for all observations assimilated in 20CRv3 at 1200 UTC on 1 June for the years (a) 1854, (b) 1915, (c) 1935, and (d) 2000. Note that comparable plots for 20CRv2c would consist entirely of light orange circles (localization value of 4000 km).

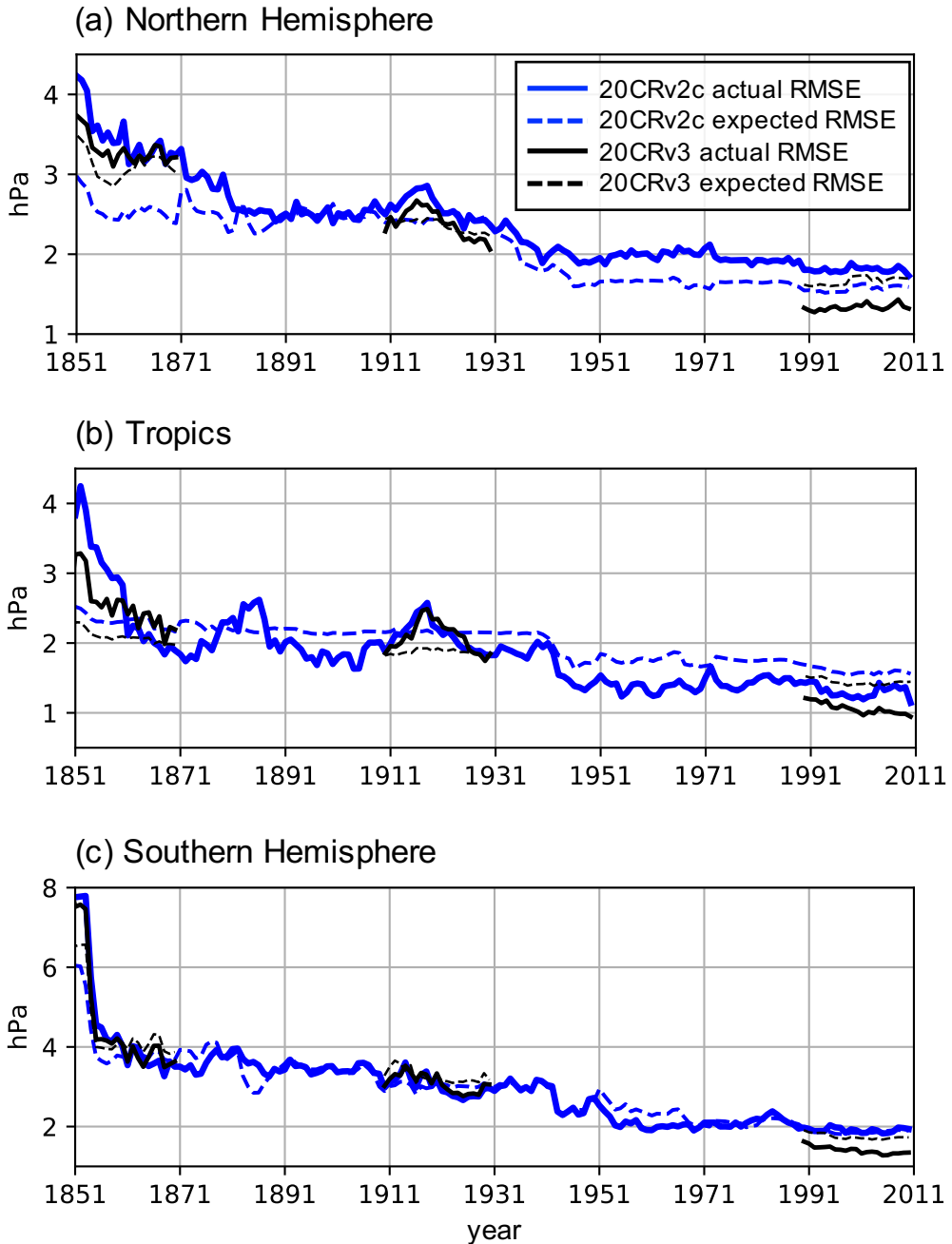


FIGURE 12 Time series of actual (solid) and expected (dashed) annual first-guess RMS errors for observations assimilated in 20CRv2c (blue) and 20CRv3 (black) averaged over (a) the Northern Hemisphere (20°N to 90°N), (b) the tropics (20°S to 20°N), and (c) the Southern Hemisphere (90°S to 20°S).

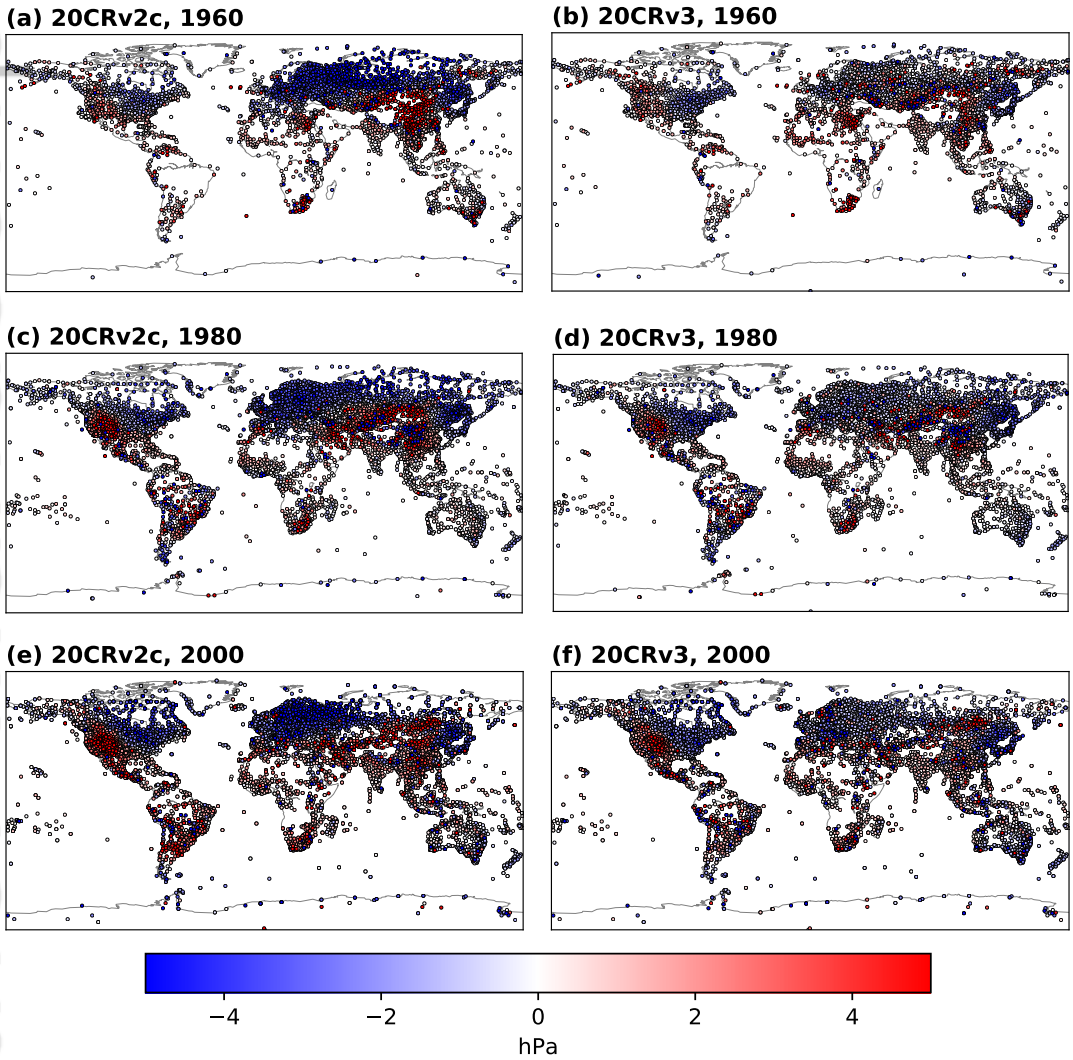


FIGURE 13 Annual average station pressure biases (hPa) for 1960 (top row), 1980 (center row), and 2000 (bottom row), calculated from 20CRv2c (left) and 20CRv3 (right).

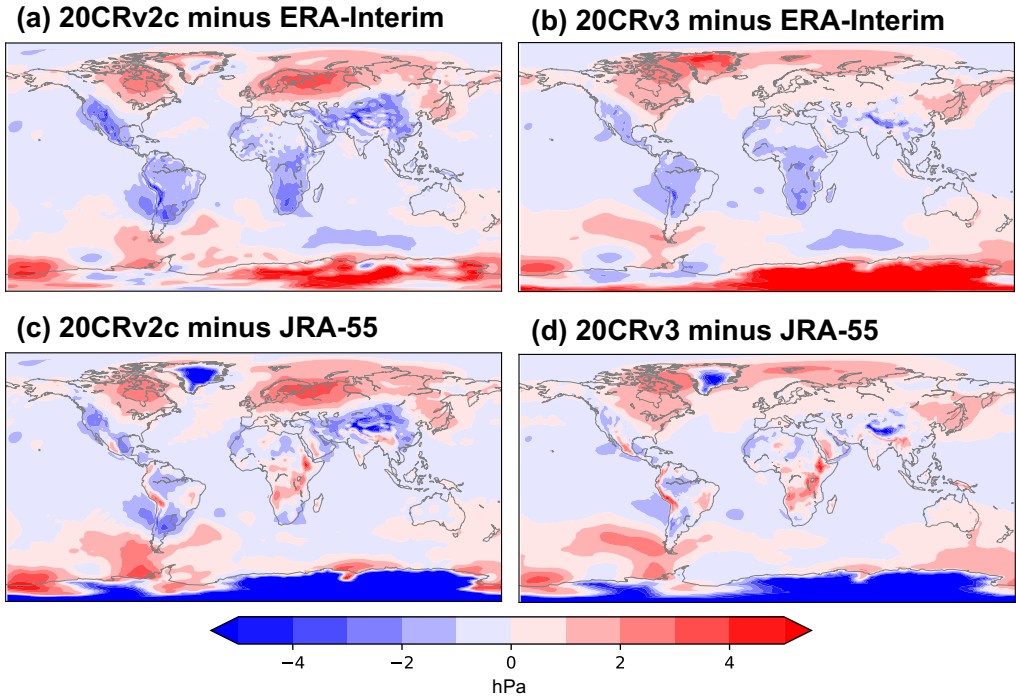


FIGURE 14 Maps of the year 2000 annually-averaged sea level pressure differences (hPa) between (a) 20CRv2c and ERA-interim, (b) 20CRv3 and ERA-interim, (c) 20CRv2c and JRA-55, and (d) 20CRv3 and JRA-55. Maps are plotted on approximately a 1.5° by 1.25° grid.

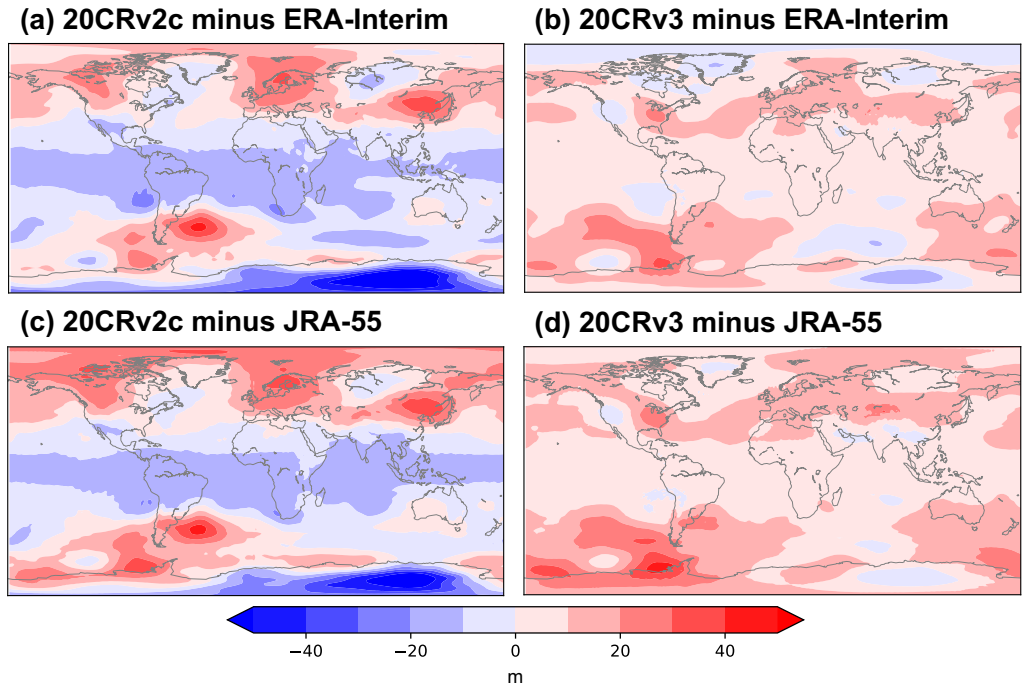
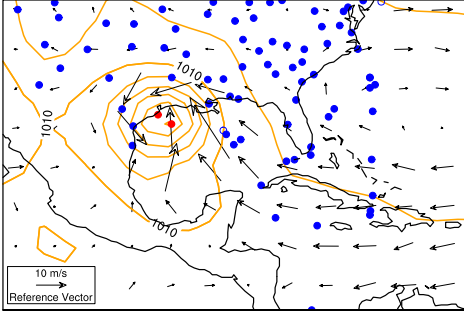
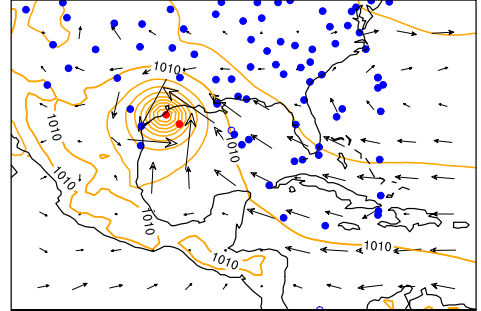


FIGURE 15 Maps of the year 2000 annually-averaged 500 hPa geopotential height differences (m) between (a) 20CRv2c and ERA-interim, (b) 20CRv3 and ERA-interim, (c) 20CRv2c and JRA-55, and (d) 20CRv3 and JRA-55. Maps are plotted on approximately a 1.5° by 1.25° grid.

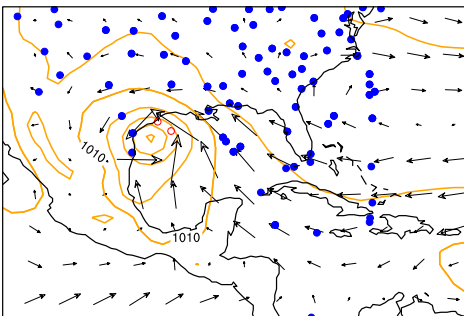
(a) 20CRv2c



(b) 20CRv3



(c) ERA-20C



(d) CERA-20C

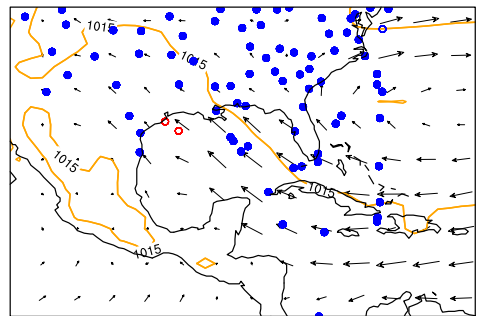


FIGURE 16 Sea level pressure (orange contours; interval by 5 hPa) and wind fields (vectors; ms^{-1}) for the 1915 Galveston hurricane, 17 Aug 1915 0600UTC, from (a) 20CRv2c, (b) 20CRv3, (c) ERA-20C, and (d) CERA-20C. Locations of available observations taken between 16 Aug 1915 2100 UTC and 17 Aug 1915 0900 UTC are shown by circles: station and marine observations are blue, IBTrACS data are red, solid circles denote observations that were assimilated, and open circles denote observations that were rejected.

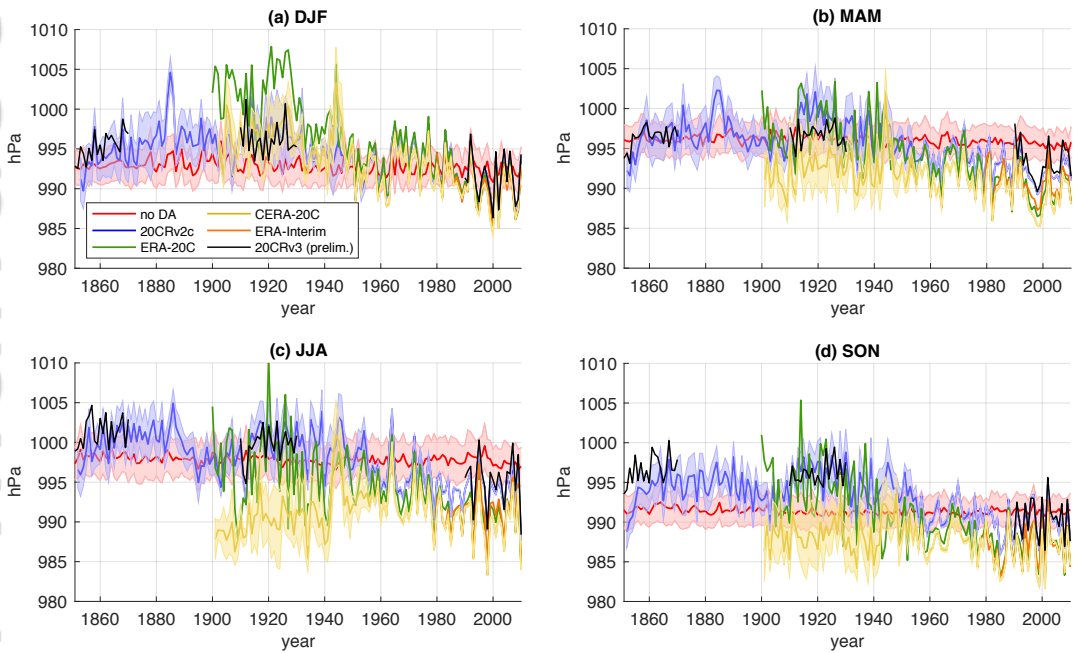


FIGURE 17 Time series of seasonal sea level pressure poleward of 60°S from 20CRv2c (blue), ERA-20C (green), CERA-20C (gold), ERA-Interim (orange), a non-assimilating model run using the 20CRv2c system (red), and preliminary 20CRv3 data without confidence intervals (black). Shading represents one ensemble standard deviation when available.

Title: Towards a more reliable historical reanalysis: Improvements for version 3 of the Twentieth Century Reanalysis system

Authors:

Laura C. Slivinski*
Gilbert P. Compo
Jeffrey S. Whitaker
Prashant D. Sardeshmukh
Benjamin S. Giese
Chesley McColl
Rob Allan
Xungang Yin
Russell Vose
Holly Titchner
John Kennedy
Lawrence J. Spencer
Linden Ashcroft
Stefan Brönnimann
Manola Brunet
Dario Camuffo
Richard Cornes
Thomas A. Cram
Richard Crouthamel
Fernando Domínguez-Castro
J. Eric Freeman
Joëlle Gergis
Ed Hawkins
Philip D. Jones
Sylvie Jourdain
Alexey Kaplan
Hisayuki Kubota
Frank Le Blancq
Tsz-Cheung Lee
Andrew Lorrey
Jürg Luterbacher
Maurizio Maugeri
Cary J. Mock
G.W. Kent Moore
Rajmund Przybylak
Christa Pudmenzky
Chris Reason
Victoria C. Slonosky
Cathy Smith
Birger Tinz
Blair Trewin

Maria Ant3nia Valente
Xiaolan L. Wang
Clive Wilkinson
Kevin Wood
Przemyslaw Wyszyński

Caption: A significant new version of the 20th Century Reanalysis data assimilation system, 20CRv3, has been developed. The 20CRv3 dataset will provide an ensemble of sub-daily global atmospheric conditions spanning over 150 years by assimilating only surface pressure observations into a coupled atmosphere-land forecast model. The new 20CRv3 system improves upon the previous system in several notable ways, including the use of upgraded data assimilation methods, a newer and higher-resolution forecast model, and a larger set of available pressure observations.

Figure:

